THE UNIVERSITY *of* EDINBURGH

# Edinburgh Research Explorer

# Feasibility Study of UAV-Assisted Anti-Jamming Positioning

OPEN ACCESS

# Feasibility Study of UAV-Assisted Anti-Jamming Positioning

Zijie Wang, Rongke Liu, *Senior Member, IEEE,* Qirui Liu, Lincong Han, and John S. Thompson, *Fellow, IEEE*

*Abstract*—As the cost and technical difficulty of jamming devices continue to decrease, jamming has become one of the major threats to positioning service. Unfortunately, most conventional wireless positioning technologies are vulnerable to jamming attacks due to inherent shortcomings like weak signal strength and unfavorable anchor geometry. Thanks to their high operational flexibility, unmanned aerial vehicles (UAVs) could be a promising solution to the above challenges. Therefore, in this article, we propose a UAV-assisted anti-jamming positioning system, in which multiple UAVs first utilize time-difference-of-arrival (TDoA) measurements from ground reference stations and double-response two-way ranging (DR-TWR) measurements from UAV-to-UAV links to perform self-localization as well as clock synchronization, and then act as anchor nodes to provide TDoA positioning service for ground users in the presence of jamming. To evaluate the feasibility and performance of the proposed system, we first derive the Cramér-Rao lower bound (CRLB) of UAV self-localization. Then, the impacts of UAV position uncertainty and synchronization errors caused by jamming on positioning service are modeled, and the theoretical root-mean-square error (RMSE) of user position estimate is further derived. Numerical results demonstrate that the proposed system is a promising alternative to existing positioning systems when their services are disrupted by jamming. The most notable advantage of the proposed system is that it is fully compatible with existing user equipment terminals and positioning methods.

*Index Terms*—Unmanned aerial vehicle (UAV), anti-jamming positioning, time-difference-of-arrival (TDoA), double-response two-way ranging (DR-TWR).

## I. INTRODUCTION

### A. Motivation

**A**S people's demand for accurate location information continues to increase, positioning technologies are playing an increasingly important role in today's society [1]. The use of positioning technologies enables a wide range of location-based services (LBS) like intelligent transport systems (ITS) and mobile marketing [2], [3], thereby promoting new developments of industrial manufacturing and our daily lives. To this end, both the fifth generation (5G) wireless networks currently under construction and the future sixth generation

(6G) networks have regarded positioning as a key technology and an essential service [4], [5]. Despite the above advantages, in practical applications, the availability and performance of positioning service can be severely affected by many factors, and jamming is one of them.

Generally speaking, jamming refers to a type of intentional radio frequency interference (RFI) emitted by hostile devices (also known as "jammer"), whose aim is to block the positioning service or degrade accuracy by disturbing the signal reception at the user equipment (UE) [6]. Due to the rapid development of the electronics industry in recent years, the cost and technical difficulty of jamming continue to decrease. A portable jammer could be easily obtained over the internet for less than 100 dollars [7]. Over the past five years, hundreds of jamming incidents have been reported around the world [8]. The frequent occurrence of jamming incidents poses serious threats to life-critical applications such as traffic management and emergency services.

Unfortunately, conventional wireless positioning technologies represented by global navigation satellite system (GNSS) and terrestrial cellular-based positioning are vulnerable to jamming attacks [9]. For the widely used GNSS systems, their services cover almost all regions of the world and could achieve centimeter-level accuracy with high-end equipment in open-sky environments [10], [11]. However, the positioning services provided by GNSS rely on satellites operating in orbit at altitudes ranging from 19 to 35 thousand km [12]. The long-distance propagation makes the strength of GNSS signals received at earth's surface extremely weak (only about -133 to -122dBm), which could be easily overwhelmed by jamming signals. In practical applications, a low-cost jammer with transmit power of 10dBm can disrupt all GNSS services within a radius of 100m [13]. Although many existing studies showed that the performance of GNSS receivers in jamming environments could be improved by adopting novel antennas or high-performance filters [14]–[16], these approaches do not change the weak signal strength, resulting in limited improvement in anti-jamming ability. Moreover, these approaches commonly require changes to the receiver's hardware or software, which means that they are cost-consuming and incompatible with existing equipment. In terms of the terrestrial cellular-based positioning, it has the ability to provide services for users in some GNSS degraded environments such as dense urban and indoors [17], [18]. Nevertheless, similar to GNSS systems, cellular-based positioning also has its own limitations. Since cellular networks are originally designed for communication applications that only require connection with one base station (BS), it is very difficult for users to find a sufficient number

of BSs for positioning [19]. Even if the user could receive signals from multiple BSs, some of them may be far away from the user, resulting in weak signals that are vulnerable to jamming attacks [20]. In addition, the geometry of terrestrial BSs is commonly unsuitable for positioning [21], which leads to large position errors even under normal conditions. Thus, the terrestrial cellular-based positioning system is likely to degrade further in the presence of jamming.

Due to the high operational flexibility and controlled mobility, low-altitude unmanned aerial vehicles (UAVs) have recently attracted increasing attention from the research community. UAVs are expected to bring a new paradigm for the design of wireless networks [22]. In the field of communication, UAVs have been studied for their ability to act as aerial BSs and relays to serve the ground users or coordinate with terrestrial networks [23]. For example, *Zhou et al.* [24], [25] designed a novel UAV-enabled mobile edge computing (MEC) system that innovatively uses UAV platform to provide computation offloading services with satisfactory security and latency for ground users. It is noteworthy that UAVs are also suitable for being employed as aerial anchor nodes to provide positioning services [26], especially in jamming environments. Compared with satellites and BSs, UAVs are capable of flying close to users, to enhance the received signal strength [27]. Besides, through the optimization of UAV deployment, users could easily establish connections with multiple UAVs, whose geometry could be adjusted flexibly according to users' requirements. Therefore, it is very promising to utilize both low-altitude UAVs and the existing terrestrial infrastructure to develop a novel anti-jamming positioning system. The aim of this study is to design such a system and evaluate its feasibility.

### B. Related Work

Due to the aforementioned advantages, UAV-enabled positioning has become a hot topic for research in recent years. The concept of using UAVs as mobile anchor nodes to locate ground users and the corresponding positioning methods were introduced in [28], [29]. In [30], [31], two UAV-enabled positioning prototypes called HAWK and GuideLoc were proposed, which employ range-free approaches to obtain rough estimates of user's location. *Sallouha et al.* [32], [33] and *Wang et al.* [34] applied the received signal strength (RSS)-based and time-difference-of-arrival (TDoA) approaches to UAV-enabled positioning to improve the accuracy of location estimation. In [35], authors performed an exhaustive survey of the positioning methods used in UAV surveillance systems, and discussed their pros and cons in detail. Furthermore, the service reliability of UAV-enabled positioning in mountainous environments was analyzed and enhanced in [36]. However, none of the above studies considered the impacts of jamming on positioning services, which renders these systems unreliable. In [37], a UAV swarm was employed to locate and track intermittent RF sources like jammers. Nevertheless, this research mainly focuses on the localization of jammers, rather than positioning services for users in jamming environments. In addition, most existing systems rely on GNSS systems to obtain the UAVs' locations, which is unrealistic in jamming

environments [13]. In [38], ground reference stations (GRSs) with known positions were used to locate UAVs, which is a potential solution to the problem of UAV self-localization in GNSS-denied environments. Nevertheless, jamming was still not taken into account in this research.

In most existing research on UAV-enabled positioning, the UAV's location information is commonly assumed to be perfectly known [32], [34]. In practice, the self-localization and clock synchronization of UAVs rely on measurements provided by satellites, GRSs or other UAVs [38], [39], which will also be inaccurate under jamming attacks. Therefore, in addition to affecting the positioning services for users, jamming will also cause anchor position and clock uncertainty in UAV-enabled positioning systems. The impact of anchor position uncertainty on RSS-based positioning systems was analyzed with Cramér-Rao lower bound (CRLB) in [40]. In [41] and [42], the CRLBs of time-of-arrival (ToA) and TDoA positioning in the presence of anchor position uncertainty were derived. The lower bound on performance in these studies can be approached by the well-known maximum-likelihood (ML) method, which is time-consuming and compute-intensive. The mean-square error (MSE) of the iterative least-squares (ILS) method derived in [43] seems to be a better metric for evaluating the position accuracy of users with low-cost equipment. However, in [43], anchor nodes were assumed to be perfectly synchronized, which may not be reasonable in multi-UAV systems. Thus, to evaluate objectively the performance of a UAV-enabled positioning system in jamming environments, both the anchor position uncertainty and clock uncertainty should be taken into consideration.

### C. Main Contributions

In this article, we propose a UAV-assisted anti-jamming positioning system consisting of multiple low-altitude UAV platforms and GRSs to provide positioning services for users in jamming environments, and theoretically analyze its performance. The proposed system takes full advantages of the high mobility and flexible aerial deployment of UAVs to improve the anti-jamming performance of positioning services. This can be achieved without using complex algorithms or changing hardware, making it fully compatible with existing low-cost equipment. Specifically, the main contributions of this article are summarized as follows.

- We establish a practical scenario in which both the UAV and ground user are affected by jamming. Compared with previous research, this scenario is more suitable for evaluating the anti-jamming performance of UAV-enabled positioning systems.
- We study the problem of UAV self-localization and clock synchronization, which has been neglected by many existing papers. A hybrid TDoA/double-response two-way ranging (DR-TWR) scheme is proposed to solve this problem, and the CRLB of UAV self-localization in the presence of jamming is derived.
- We use the TDoA measurements provided by UAVs and ILS method to locate users. The impact of UAV position and clock uncertainty on the positioning service
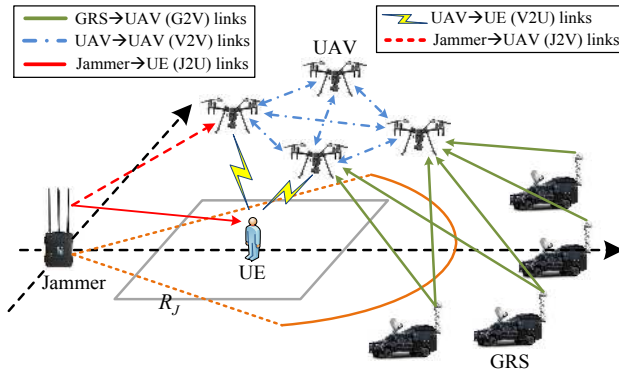
Fig. 1. Proposed UAV-assisted anti-jamming positioning system.

is analyzed, and the theoretical root-mean-square error (RMSE) of user position estimate is derived. Compared with metrics used in existing research, RMSE is more appropriate for describing the position accuracy of low-cost UE in UAV-enabled positioning systems.

The remainder of this article is organized as follows. The structure of the proposed system and the positioning methods used are given in Section II. Section III derives the CRLB of UAV self-localization and the RMSE of UE position estimate in jamming environments. Section IV provides numerical results to demonstrate the feasibility and validity of our proposed system. Finally, Section V concludes this article.

The main notations used in this article are summarized as follows. Scalars are denoted by italic letters ($a$). Column vectors and matrices are denoted by lowercase and uppercase boldface letters ($\mathbf{a}$ and $\mathbf{A}$), respectively. The superscript $T$ indicates the transpose operation ($\mathbf{A}^T$) and superscript $-1$ indicates matrix inverse ($\mathbf{A}^{-1}$). $\|\cdot\|$ represents the Euclidean norm of a vector.

## II. SYSTEM DESIGN

In this article, as shown in Fig. 1, we consider a scenario consisting of a portable jammer, $M$ mobile GRSs and $N$ low-altitude UAV platforms. GRSs and UAVs are denoted by sets $\mathcal{G} \triangleq \{G_1, G_2, \cdots, G_M\}$ and $\mathcal{V} \triangleq \{V_1, V_2, \cdots, V_N\}$, respectively. The location of the jammer has been accurately measured in advance and is denoted by the horizontal coordinates $\mathbf{w} = (x_J, y_J)^T \in \mathbb{R}^{2 \times 1}$ and height $h_J$. Its three-dimensional (3-D) location is denoted by $\mathbf{w}_{3D} = \left[\mathbf{w}^T, h_J\right]^T$. The jammer continuously emits noise-like jamming signals in GNSS and 2.4 GHz ISM bands, blocking the reception of all GNSS signals within $R_J$ meters around it. This circular area in which GNSS services are completely disrupted is called the "jamming area", whose boundary is indicated by the brown solid line in Fig. 1. In addition, it is assumed that the jammer has the ability to identify and track the frequency of positioning signals, so that the jamming cannot be mitigated by transmitting signals at different frequencies. The transmit power of the jammer in the ISM band is denoted by $P_J^t$.

A mobile GRS could be an autonomous land vehicle (ALV) equipped with a high-end GNSS receiver as well as an ISM band transceiver. The former is used to determine the

GRS's own location, while the latter is used for providing positioning services. In order to receive GNSS signals and locate itself, each GRS must stay at least $R_J$ meters away from the jammer, that is, outside the jamming area. Moreover, we assume that if this requirement is satisfied, the impact of jamming on GRSs' position accuracy can be effectively mitigated. The location of the $m$-th GRS ($G_m$) is denoted by the horizontal coordinates $\mathbf{g}_m = (x_G^m, y_G^m)^T \in \mathbb{R}^{2 \times 1}$ and height $h_G$ ($\mathbf{g}_{m,3D} = \left[\mathbf{g}_m^T, h_G\right]^T$). $P_G^t$ is the transmit power of its ISM band transceiver.

UEs that are denied positioning services due to jamming are located in a square area called the "target area", which is marked in grey in Fig. 1. The center and side length of the target area are denoted by $\mathbf{o}_T$ and $L_T$, respectively. It is assumed that UEs are uniformly distributed within the target area. The true location of each UE is denoted by $\mathbf{u}^* = (x_U^*, y_U^*)^T \in \mathbb{R}^{2 \times 1}$, and its height $h_U$ is set to 1.5m ($\mathbf{u}_{3D}^* = \left[(\mathbf{u}^*)^T, h_U\right]^T$), which is the average height of handheld devices. As can be seen from Fig. 1, the target area is inside the jamming area, which means that UEs cannot use GNSS systems to locate themselves. As mentioned above, GRSs have to stay outside the jamming area, which means they are further away from UEs. Thus, the probability that LoS paths exist between GRSs and UEs is extremely low. Moreover, in order to maintain the connection with the controller, GRSs are commonly not far apart, resulting in an unfavorable geometry for positioning. From the above analysis, it can be concluded that GRSs are also unsuitable for providing positioning services for UEs in the target area.

In order to meet UEs' requirements for positioning services, we introduce UAVs into this scenario and form a novel anti-jamming positioning system together with the existing GRSs. Similar to UEs, UAVs hovering at a fixed altitude $h_V$ over the jamming area cannot use GNSS systems to determine their own locations. Compared with weak GNSS signals, the ISM band signals transmitted by low-altitude or ground platforms at higher power are less likely to be overwhelmed by jamming signals. Thus, each UAV is equipped with an ISM band transceiver, which will be used to establish wireless links with the GRSs, other UAVs and UEs for self-localization as well as providing positioning services. The true location of the $n$-th UAV ($V_n$) is denoted by the horizontal coordinates $\mathbf{v}_n^* = (x_V^{n*}, y_V^{n*})^T \in \mathbb{R}^{2 \times 1}$ and height $h_V$ ($\mathbf{v}_{n,3D}^* = \left[(\mathbf{v}_n^*)^T, h_V\right]^T$). The transmit power of its ISM band transceiver is denoted by $P_V^t$. In the proposed system, the UAVs first utilize the measurements obtained from GRS-to-UAV (G2V) and UAV-to-UAV (V2V) links to perform self-localization and clock synchronization. After their own locations are determined, these UAVs will be used as anchor nodes to provide positioning services for UEs through UAV-to-UE (V2U) links. Both the UAV self-localization process and service process are affected by jamming. Since UAVs can move close to UEs and maintain a satisfactory geometry for positioning, the proposed system is expected to achieve good anti-jamming performance.

### A. Hybrid TDoA/DR-TWR UAV Self-Localization

As shown in Fig. 1, in the proposed system, each UAV $V_n$ could use its ISM band transceiver to establish $M$ G2V
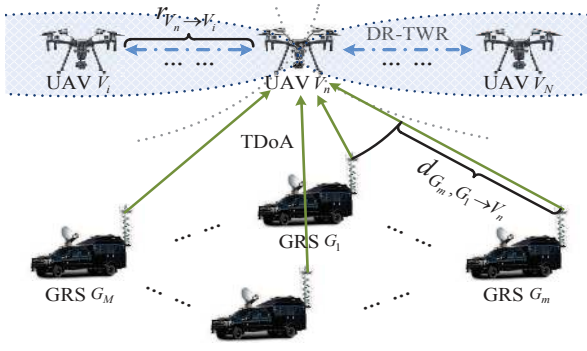
Fig. 2. Model of UAV self-localization.

measurement links and $(N-1)$ V2V measurement links. Moreover, there is also a Jammer-to-UAV (J2V) jamming link between the jammer and each UAV. These three kinds of wireless links can be characterized with two types of channels, namely the Ground-to-Air (G2A) channel and the Air-to-Air (A2A) channel. The former includes the G2V and J2V links, while the V2V links belong to the latter. The G2V links are assumed to be dominated by LoS components. This assumption is quite reasonable because the high altitude of UAVs commonly leads to a high probability of LoS propagation [44], [45]. Then, the average path loss between GRS $G_m$ and UAV $V_n$ can be expressed as

$$PL_{G_m \to V_n} = \beta_0 \big( \| \mathbf{v}_{n,3D}^* - \mathbf{g}_{m,3D} \| \big)^{\alpha_{G2A}^L}, \qquad (1)$$

where $\beta_0 = \left( \frac{4\pi f_c}{c} \right)^2$ is the reference path loss at a distance of 1m; $f_c$ and $c$ are the main frequency of the ISM band transceiver (2.4GHz) and the speed of light, respectively. $\alpha_{G2A}^L$ is the path loss exponent (PLE) of the G2A channel under LoS conditions.

Moreover, we also assume that there are always clear LoS paths between UAVs [46]. Therefore, the path loss between UAV $V_n$ and $V_i$ follows the free space propagation model and can be written as

$$PL_{V_i \to V_n} = \beta_0 \big( \| \mathbf{v}_{n.3D}^* - \mathbf{v}_{i,3D}^* \| \big)^2. \qquad (2)$$

Different from G2V links, the propagation condition of the J2V link could be either LoS or NLoS. The NLoS condition occurs when the UAV chooses to hide behind obstructions like buildings or mountains to reduce the impact of jamming on its signal reception. Then, the average path loss between the jammer and UAV $V_n$ can be expressed as

$$PL_{J \to V_n} = \beta_0 \big( \| \mathbf{v}_{n,3D}^* - \mathbf{w}_{3D} \| \big)^{\alpha_{G2A}^X}, \qquad (3)$$

where the superscript $X$ of $\alpha_{G2A}^X$ is either L or N, indicating the propagation condition (LoS or NLoS). Please note that the small-scale channel fading is not considered in the above equation because it can be averaged out using positioning signals with large frame length [47], [48].

The signal-to-interference-plus-noise ratios (SINR) of the positioning signals transmitted by GRS $G_m$ and UAV $V_i$ at UAV $V_n$ can be expressed as follows:

$$SINR_{G_m \to V_n} = \frac{P_G^t / PL_{G_m \to V_n}}{P_{n_0} + P_J^t / PL_{J \to V_n}}, \qquad (4)$$

$$SINR_{V_i \to V_n} = \frac{P_V^t / PL_{V_i \to V_n}}{P_{n_0} + P_J^t / PL_{J \to V_n}}, \qquad (5)$$

where $P_{n_0}$ is the noise power. As described in [49], the minimum variances of ToA measurements that UAV $V_n$ could achieve are given by

$$\sigma_{G_m \to V_n}^2 \, (m^2) = c^2 / \big( B^2 \cdot SINR_{G_m \to V_n} \big), \qquad (6)$$

$$\sigma_{V_i \to V_n}^2 \, (m^2) = c^2 / \big( B^2 \cdot SINR_{V_i \to V_n} \big), \qquad (7)$$

where $B$ is the signal bandwidth. As shown in Fig. 2, UAVs utilize two types of measurements to estimate their own locations, one of which is the TDoA measurement obtained through G2V links. Since GRSs have been accurately synchronized with each other using GNSS systems, measuring the TDoA between a pair of GRSs could eliminate the unknown clock bias between GRSs and the UAV. Let GRS $G_1$ be the reference node, the TDoA measurement of GRS pair $\langle G_m, G_1 \rangle$ measured at UAV $V_n$ can be expressed as

$$\begin{aligned} d_{G_m,G_1 \to V_n} &= \| \mathbf{v}_{n3D}^* - \mathbf{g}_{m3D} \| - \| \mathbf{v}_{n3D}^* - \mathbf{g}_{13D} \| + n_{G_m G_1 \to V_n} \\ &= r_{G_m \to V_n}^* - r_{G_1 \to V_n}^* + n_{G_m,G_1 \to V_n} \\ &= d_{G_m,G_1 \to V_n}^* + n_{G_m,G_1 \to V_n}, \end{aligned}$$
(8)

where $d_{G_m,G_1 \to V_n}^*$ denotes the true TDoA of the GRS pair $\langle G_m, G_1 \rangle$; $r_{G_m \to V_n}^*$ $(r_{G_1 \to V_n}^*)$ is the true distance between GRS $G_m$ $(G_1)$ and UAV $V_n$; $n_{G_m,G_1 \to V_n} \sim \mathcal{N}\big( 0, \sigma_{G_m \to V_n}^2 + \sigma_{G_1 \to V_n}^2 \big)$ is the TDoA measurement error caused by transceiver's internal noise and jamming.

Through G2V links, each UAV $V_n$ could collect $(M-1)$ TDoA measurements, which can be represented by the following vector:

$$\begin{aligned} \mathbf{d}_{G \to V_n} &= [d_{G_2,G_1 \to V_n}, \cdots, d_{G_M,G_1 \to V_n}]^T \\ &= \mathbf{d}_{G \to V_n}^* + \mathbf{n}_{G \to V_n}, \end{aligned}$$
(9)

where the vector $\mathbf{d}_{G \to V_n}^* = \left[ d_{G_2,G_1 \to V_n}^*, \cdots, d_{G_M,G_1 \to V_n}^* \right]^T$ denotes the true values of the $(M-1)$ TDoA measurements, and $\mathbf{n}_{G \to V_n} = [n_{G_2,G_1 \to V_n}, \cdots, n_{G_M,G_1 \to V_n}]^T$ is the vector of measurement errors. The total TDoA measurements collected by $N$ UAVs form the following $N(M-1) \times 1$ vector:

$$\mathbf{d}_{G \to V} = \big[ \mathbf{d}_{G \to V_1}^T, \cdots, \mathbf{d}_{G \to V_N}^T \big]^T = \mathbf{d}_{G \to V}^* + \mathbf{n}_{G \to V}, \quad (10)$$

where $\mathbf{d}_{G \to V}^* = \left[ \big( \mathbf{d}_{G \to V_1}^* \big)^T, \cdots, \big( \mathbf{d}_{G \to V_N}^* \big)^T \right]^T$ and $\mathbf{n}_{G \to V} = \left[ \mathbf{n}_{G \to V_1}^T, \cdots, \mathbf{n}_{G \to V_N}^T \right]^T$.

The other type of measurements for UAV self-localization is the range measurement obtained with DR-TWR technique through V2V links. DR-TWR technique can ease the constraint of clock synchronization through the exchange of messages [50], making it suitable for measuring the range between two UAVs before they are synchronized. As shown in Appendix A, the DR-TWR measurement corresponding to UAV pair $\langle V_n, V_i \rangle$ $(i \neq n)$ and obtained at UAV $V_n$ can be expressed as

$$r_{V_n \to V_i} = r_{V_n \to V_i}^* + n_{V_n \to V_i} = \| \mathbf{v}_n^* - \mathbf{v}_i^* \| + n_{V_n \to V_i}, \quad (11)$$

where $r_{V_n \to V_i}^*$ denotes the true range between UAV $V_n$ and $V_i$; $n_{V_n \to V_i} \sim \mathcal{N}\big( 0, \frac{1}{4}\sigma_{V_n \to V_i}^2 + \frac{5}{4}\sigma_{V_i \to V_n}^2 \big)$ is the total range

measurement error caused by 1) transceivers' internal noise and 2) jamming.

Let $\mathcal{L}_n \triangleq \{1, \cdots, n-1, n+1, \cdots, N\}$, and $L_{n,i}$ represents the $i$-th element in set $\mathcal{L}_n$. Then, the $(N-1)$ DR-TWR range measurements collected by UAV $V_n$ can be represented by the vector:

$$
\begin{aligned}
\mathbf{r}_{V_n \to V} &= \left[ r_{V_n \to V_{L_{n,1}}}, \cdots, r_{V_n \to V_{L_{n,N-1}}} \right]^T \\
&= \mathbf{r}^*_{V_n \to V} + \mathbf{n}_{V_n \to V},
\end{aligned}
\tag{12}
$$

where the vector $\mathbf{r}^*_{V_n \to V} = \left[ r^*_{V_n \to V_{L_{n,1}}}, \cdots, r^*_{V_n \to V_{L_{n,N-1}}} \right]^T$ denotes the true values of $(N-1)$ range measurements, and $\mathbf{n}_{V_n \to V} = \left[ n_{V_n \to V_{L_{n,1}}}, \cdots, n_{V_n \to V_{L_{n,N-1}}} \right]^T$ is the vector of measurement errors. The total $N \times (N-1)$ range measurements obtained by the $N$ UAVs form the following vector:

$$
\mathbf{r}_{V \to V} = \left[ \mathbf{r}^T_{V_1 \to V}, \cdots, \mathbf{r}^T_{V_N \to V} \right]^T = \mathbf{r}^*_{V \to V} + \mathbf{n}_{V \to V}.
\tag{13}
$$

Putting the measurement vectors $\mathbf{d}_{G \to V}$ and $\mathbf{r}_{V \to V}$ together, the total $N \times (M+N-2)$ measurements obtained by UAVs can be represented by the vector:

$$
\mathbf{o}_V = \left[ \mathbf{d}^T_{G \to V}, \mathbf{r}^T_{V \to V} \right]^T = \mathbf{o}^*_V + \mathbf{n}_V,
\tag{14}
$$

where $\mathbf{o}^*_V = \left[ (\mathbf{d}^*_{G \to V})^T, (\mathbf{r}^*_{V \to V})^T \right]^T$, $\mathbf{n}_V = \left[ \mathbf{n}^T_{G \to V}, \mathbf{n}^T_{V \to V} \right]^T$. The parameters to be estimated in the UAV self-localization process are the horizontal coordinates of $N$ UAVs, which can be denoted as

$$
\mathbf{v} = \left[ \mathbf{v}^T_1, \cdots, \mathbf{v}^T_N \right]^T = \left[ x^1_V, y^1_V, \cdots, x^N_V, y^N_V \right]^T.
\tag{15}
$$

In the proposed system, UAVs send all their measurements ($\mathbf{o}_V$) to GRS $G_1$, which will use the well-known ML method to estimate UAVs' locations ($\mathbf{v}$). The estimated locations are denoted by vector $\hat{\mathbf{v}} = \left[ \hat{\mathbf{v}}^T_1, \cdots, \hat{\mathbf{v}}^T_N \right]^T$.

### B. Clock Synchronization between UAVs

To be employed as anchor nodes for TDoA positioning, UAVs need to be clock synchronized. In the proposed system, the local clock of GRS $G_1$ that has already been synchronized with GNSS is treated as the reference clock for timing services. During the mission, GRS $G_1$ periodically sends synchronization messages with timestamps to UAVs. The synchronization message sent at time $t_s$ will be detected by UAV $V_n$ at time

$$
t^*_{r,n} = t_s + \left( r^*_{G_1 \to V_n} + e_{G_1 \to V_n} \right) / c,
\tag{16}
$$

where $e_{G_1 \to V_n} \sim \mathcal{N}\left( 0, \sigma^2_{G_1 \to V_n} \right)$ denotes the synchronization error (m) caused by transceiver's internal noise and jamming.

For UAV $V_n$, the transmission time $t_s$ of the synchronization message can be extracted from the received timestamp, while the true range $r^*_{G_1 \to V_n}$ is unavailable. Replacing $r^*_{G_1 \to V_n}$ in equation (16) with the predicted range $\hat{r}_{G_1 \to V_n}$ based on the estimated location $\hat{\mathbf{v}}_{n,3D} = \left[ \hat{\mathbf{v}}^T_n, h_V \right]^T$, the synchronization result at UAV $V_n$ can be expressed as

$$
\hat{t}_{r,V_n} = t_s + \frac{\hat{r}_{G_1 \to V_n}}{c} = t_s + \frac{\| \hat{\mathbf{v}}_{n,3D} - \mathbf{g}_{1,3D} \|}{c}.
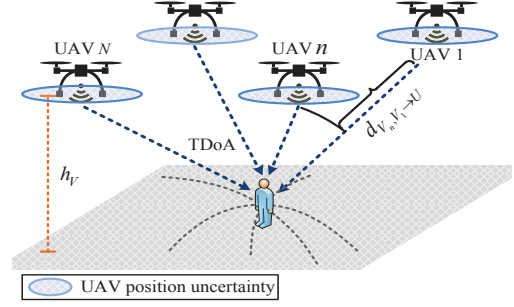\tag{17}
$$



Fig. 3. Model of UE Positioning.

Then, the clock synchronization error (m) corresponding to UAV $V_n$ can be written as

$$
\begin{aligned}
\Delta t_{V_n} &= c \cdot \left( \hat{t}_{r,V_n} - t^*_{r,V_n} \right) = \hat{r}_{G_1 \to V_n} - r^*_{G_1 \to V_n} + e_{G_1 \to V_n} \\
&= \| \hat{\mathbf{v}}_{n,3D} - \mathbf{g}_{1,3D} \| - \| \mathbf{v}^*_{n,3D} - \mathbf{g}_{1,3D} \| + e_{G_1 \to V_n}.
\end{aligned}
\tag{18}
$$

It can be clearly seen from the above equation that the clock synchronization error consists of two components, that is, the range prediction error caused by UAV position uncertainty and the ToA measurement error caused by internal noise and jamming.

### C. TDoA Positioning Services for UE

After their time and locations are determined by the schemes introduced in the previous subsections, UAVs in the proposed system will be used as anchor nodes to provide positioning services for UEs. As shown in Fig. 1, each UE could receive positioning signals from UAVs through $N$ UAV-to-UE (V2U) measurement links. Similar to UAVs, the signal reception at the UE is also affected by the Jammer-to-UE (J2U) jamming link. The V2U links can be modeled as G2A channels, and their propagation conditions are assumed to be LoS [45]. Thus, the average path loss $PL_{V_n \to U}$ between the UE and UAV $V_n$ can be calculated by replacing $\mathbf{g}_{m,3D}$ in equation (1) with $\mathbf{u}^*_{3D}$. The J2U jamming link is a typical Ground-to-Ground (G2G) channel. Since the jammer is close to the UE, the J2U link is assumed to be dominated by the LoS component [21], and its average path loss can be expressed as

$$
PL_{J \to U} = \beta_0 (\| \mathbf{u}^*_{3D} - \mathbf{w}_{3D} \|)^{\alpha^L_{G2G}},
\tag{19}
$$

where $\alpha^L_{G2G}$ denotes the PLE of the G2G channel under LoS conditions. Then, the SINR ($SINR_{V_n \to U}$) and ToA measurement variance ($\sigma^2_{V_n \to U}$) at the UE can be calculated with approaches similar to equations (4) and (6).

As shown in Fig. 3, we use the TDoA technique to support positioning services. The reason for choosing TDoA is that this technique has been widely adopted in many existing systems such as the Long Term Evolution (LTE) networks, so that the services provided by the proposed system can be fully compatible with existing equipment. Let UAV $V_1$ be the reference node, the TDoA measurement of the UAV pair $\langle V_n, V_1 \rangle$ measured at the UE can be written as equation (20), where $d^*_{V_n, V_1 \to U}$ denotes the true value of the TDoA measurement; $\Delta t^{Pos}_{V_n, V_1 \to U} = \left( \hat{r}_{G_1 \to V_n} - r^*_{G_1 \to V_n} \right) - \left( \hat{r}_{G_1 \to V_1} - r^*_{G_1 \to V_1} \right)$ and $\Delta t^{Noi}_{V_n, V_1 \to U} = \left( e_{G_1 \to V_n} - e_{G_1 \to V_1} \right) \sim \mathcal{N}\left( 0, \sigma^2_{G_1 \to V_n} + \sigma^2_{G_1 \to V_1} \right)$

$$\begin{aligned}
d_{V_n,V_1 \to U} &= \left\| \mathbf{u}_{3D}^* - \mathbf{v}_{n,3D}^* \right\| - \left\| \mathbf{u}_{3D}^* - \mathbf{v}_{1,3D}^* \right\| - (\Delta t_{V_n} - \Delta t_{V_1}) + n_{V_n,V_1 \to U} \\
&= d_{V_n,V_1 \to U}^* - \left[ (\hat{r}_{G_1 \to V_n} - r_{G_1 \to V_n}^*) - (\hat{r}_{G_1 \to V_1} - r_{G_1 \to V_1}^*) \right] - (e_{G_1 \to V_n} - e_{G_1 \to V_1}) + n_{V_n,V_1 \to U} \\
&= d_{V_n,V_1 \to U}^* - \Delta t_{V_n,V_1 \to U}^{Pos} - \Delta t_{V_n,V_1 \to U}^{Noi} + n_{V_n,V_1 \to U}.
\end{aligned} \tag{20}$$

indicate the impacts of clock synchronization errors caused by UAV position uncertainty and jamming on the TDoA measurement, respectively; $n_{V_n,V_1 \to U} \sim \mathcal{N}\left(0, \sigma_{V_n \to U}^2 + \sigma_{V_1 \to U}^2\right)$ is the measurement error caused by UE's internal noise and jamming.

The UE could collect $(N-1)$ TDoA measurements through V2U links, which can be represented by the following vector:

$$\begin{aligned}
\mathbf{d}_{V \to U} &= [d_{V_2,V_1 \to U}, \cdots, d_{V_N,V_1 \to U}]^T \\
&= \mathbf{d}_{V \to U}^* - \Delta \mathbf{t}_{V \to U}^{Pos} - \Delta \mathbf{t}_{V \to U}^{Noi} + \mathbf{n}_{V \to U},
\end{aligned} \tag{21}$$

where

$$\mathbf{d}_{V \to U}^* = \left[d_{V_2,V_1 \to U}^*, \cdots, d_{V_N,V_1 \to U}^*\right]^T, \tag{22}$$

$$\Delta \mathbf{t}_{V \to U}^{Pos} = \left[\Delta t_{V_2,V_1 \to U}^{Pos}, \cdots, \Delta t_{V_N,V_1 \to U}^{Pos}\right]^T, \tag{23}$$

$$\Delta \mathbf{t}_{V \to U}^{Noi} = \left[\Delta t_{V_2,V_1 \to U}^{Noi}, \cdots, \Delta t_{V_N,V_1 \to U}^{Noi}\right]^T, \tag{24}$$

$$\mathbf{n}_{V \to U} = \left[n_{V_2,V_1 \to U}, \cdots, n_{V_N,V_1 \to U}\right]^T. \tag{25}$$

After collecting all the TDoA measurements in vector $\mathbf{d}_{V \to U}$, the horizontal coordinates ($\mathbf{u} = [x_U, y_U]^T$) of the UE could be estimated with the widely used ILS method. The estimated UE location is denoted by vector $\hat{\mathbf{u}} = [\hat{x}_U, \hat{y}_U]^T$.

## III. THEORETICAL ANALYSIS OF PERFORMANCE

In this section, we evaluate the theoretical performance of the proposed system under jamming attacks. Different from previous studies in which the UAVs' locations are assumed to be perfectly known [32], [34], we consider the impacts of jamming on both UAV self-localization and UE position estimation, making the evaluation results more practical. Specifically, the CRLB of the proposed hybrid TDoA/DR-TWR UAV self-localization scheme is first derived in subsection A. Then, in subsection B, we derive the RMSE of UE position estimate in the presence of UAV position and clock uncertainty. Finally, in subsection C, we analyze some other performance metrics that need to be considered in real-world applications.

### A. CRLB of UAV Self-Localization

As mentioned in Section II.A, during the UAV self-localization process, GRS $G_1$ with sufficient computation power will use the ML method to determine periodically the UAVs' locations. Thus, the CRLB that could be approached by ML method is used to indicate the theoretical performance of UAV self-localization in the presence of jamming. Since the TDoA vector $\mathbf{d}_{G \to V}$ and DR-TWR vector $\mathbf{r}_{V \to V}$ are independent of each other, the log-likelihood function of the measurement vector $\mathbf{o}_V$ can be expressed as

$$\ln f\left(\mathbf{o}_V; \mathbf{v}\right) = \ln f\left(\mathbf{d}_{G \to V}; \mathbf{v}\right) + \ln f\left(\mathbf{r}_{V \to V}; \mathbf{v}\right), \tag{26}$$

where $f\left(\mathbf{d}_{G \to V}; \mathbf{v}\right)$ and $f\left(\mathbf{r}_{V \to V}; \mathbf{v}\right)$ are likelihood functions of TDoA measurements and DR-TWR measurements, respectively. The expressions of $f\left(\mathbf{d}_{G \to V}; \mathbf{v}\right)$ and $f\left(\mathbf{r}_{V \to V}; \mathbf{v}\right)$ are

$$\begin{aligned}
f\left(\mathbf{d}_{G \to V}; \mathbf{v}\right) &= \left((2\pi)^{N(M-1)} \left|\mathbf{Q}_{\mathbf{n}_{G \to V}}\right|\right)^{\frac{1}{2}} \\
&\cdot \exp\left(-\frac{1}{2}(\mathbf{d}_{G \to V} - \mathbf{d}_{G \to V}^*)^T \mathbf{Q}_{\mathbf{n}_{G \to V}}^* (\mathbf{d}_{G \to V} - \mathbf{d}_{G \to V}^*)\right),
\end{aligned} \tag{27}$$

$$\begin{aligned}
f\left(\mathbf{r}_{V \to V}; \mathbf{v}\right) &= \left((2\pi)^{N(N-1)} \left|\mathbf{Q}_{\mathbf{n}_{V \to V}}\right|\right)^{\frac{1}{2}} \\
&\cdot \exp\left(-\frac{1}{2}(\mathbf{r}_{V \to V} - \mathbf{r}_{V \to V}^*)^T \mathbf{Q}_{\mathbf{n}_{V \to V}}^* (\mathbf{r}_{V \to V} - \mathbf{r}_{V \to V}^*)\right),
\end{aligned} \tag{28}$$

where $\mathbf{Q}_{\mathbf{n}_{G \to V}}$ and $\mathbf{Q}_{\mathbf{n}_{V \to V}}$ are the covariance matrices of TDoA error vector $\mathbf{n}_{G \to V}$ and DR-TWR error vector $\mathbf{n}_{V \to V}$, respectively. Their expressions can be written as

$$\mathbf{Q}_{\mathbf{n}_{G \to V}} = \text{cov}\left(\mathbf{n}_{G \to V}\right) = \text{blkdiag}\left(\mathbf{Q}_{\mathbf{n}_{G \to V_1}}, \cdots, \mathbf{Q}_{\mathbf{n}_{G \to V_N}}\right), \tag{29}$$

$$\mathbf{Q}_{\mathbf{n}_{V \to V}} = \text{cov}\left(\mathbf{n}_{V \to V}\right) = \text{blkdiag}\left(\mathbf{Q}_{\mathbf{n}_{V_1 \to V}}, \cdots, \mathbf{Q}_{\mathbf{n}_{V_N \to V}}\right), \tag{30}$$

where $\text{blkdiag}(\cdot)$ denotes the block diagonal matrix, and

$$\mathbf{Q}_{\mathbf{n}_{G \to V_n}} = \sigma_{G_1 \to V_n}^2 \cdot \mathbf{I}_{M-1} + \text{diag}\left(\sigma_{G_2 \to V_n}^2, \cdots, \sigma_{G_M \to V_n}^2\right), \tag{31}$$

$$\mathbf{Q}_{\mathbf{n}_{V_n \to V}} = \text{diag}\left(\sigma_{V_n \to V_{L_{n,1}}}^2, \cdots, \sigma_{V_n \to V_{L_{n,N-1}}}^2\right), \tag{32}$$

and $\mathbf{I}_{M-1}$ denotes the $(M-1) \times (M-1)$ identity matrix.

Then, the CRLB for UAV location estimation can be calculated using the following equation:

$$\begin{aligned}
\text{CRLB}\left(\mathbf{v}\right) &= -E\left[\frac{\partial^2 \ln f\left(\mathbf{o}_V; \mathbf{v}\right)}{\partial \mathbf{v} \partial \mathbf{v}^T}\right]^{-1} \\
&= -E\left[\frac{\partial^2 \ln f\left(\mathbf{d}_{G \to V}; \mathbf{v}\right)}{\partial \mathbf{v} \partial \mathbf{v}^T} + \frac{\partial^2 \ln f\left(\mathbf{r}_{G \to G}; \mathbf{v}\right)}{\partial \mathbf{v} \partial \mathbf{v}^T}\right]^{-1} \\
&= \left[\underbrace{\left(\frac{\partial \mathbf{d}_{G \to V}^*}{\partial \mathbf{v}}\right)^T \mathbf{Q}_{\mathbf{n}_{G \to V}}^{-1} \left(\frac{\partial \mathbf{d}_{G \to V}^*}{\partial \mathbf{v}}\right)}_{\mathbf{J}_{G \to V}^{\text{TDoA}}} \right. \\
&\quad \left. + \underbrace{\left(\frac{\partial \mathbf{r}_{V \to V}^*}{\partial \mathbf{v}}\right)^T \mathbf{Q}_{\mathbf{n}_{V \to V}}^{-1} \left(\frac{\partial \mathbf{r}_{V \to V}^*}{\partial \mathbf{v}}\right)}_{\mathbf{J}_{V \to V}^{\text{DR-TWR}}}\right]^{-1},
\end{aligned} \tag{33}$$

where $\mathbf{J}_{G \to V}^{\text{TDoA}}$ and $\mathbf{J}_{V \to V}^{\text{DR-TWR}}$ are Fisher information matrices (FIM) corresponding to G2V TDoA measurements and V2V DR-TWR measurements, respectively. It can be clearly seen from the above equation that the CRLB is the inverse of the sum of FIM $\mathbf{J}_{G \to V}^{\text{TDoA}}$ and $\mathbf{J}_{V \to V}^{\text{DR-TWR}}$, which reflects the

$$\mathbf{R}_n\left(i,:\right) = \frac{\partial r_{V_n \to V_{L_{n,i}}}^*}{\partial \mathbf{v}} = \begin{cases} \left[\mathbf{0}_{2(L_{n,i}-1)\times 1}^T, -\left(\mathbf{k}_{\mathbf{v}_{L_{n,i}}^*}^{\mathbf{v}_n^*}\right)^T, \mathbf{0}_{2(n-L_{n,i}-1)\times 1}^T, \left(\mathbf{k}_{\mathbf{v}_{L_{n,i}}^*}^{\mathbf{v}_n^*}\right)^T, \mathbf{0}_{2(N-n)\times 1}^T\right], & \text{if } L_{n,i} < n, \\ \left[\mathbf{0}_{2(n-1)\times 1}^T, \left(\mathbf{k}_{\mathbf{v}_{L_{n,i}}^*}^{\mathbf{v}_n^*}\right)^T, \mathbf{0}_{2(L_{n,i}-n-1)\times 1}^T, -\left(\mathbf{k}_{\mathbf{v}_{L_{n,i}}^*}^{\mathbf{v}_n^*}\right)^T, \mathbf{0}_{2(N-L_{n,i})\times 1}^T\right], & \text{if } L_{n,i} \geq n, \end{cases} \quad (38)$$

contribution of the two types of measurements to position accuracy. $\frac{\partial \mathbf{d}_{G\to V}^*}{\partial \mathbf{v}}$ in equation (33) is the partial derivative of TDoA measurements with respect to the UAVs' locations, which can be expressed as

$$\frac{\partial \mathbf{d}_{G\to V}^*}{\partial \mathbf{v}} = \text{blkdiag}\left(\mathbf{D}_1, \mathbf{D}_2, \cdots, \mathbf{D}_N\right), \quad (34)$$

where $\mathbf{D}_n$ is a $(M-1)\times 2$ matrix, whose expression can be written as $(1 \leq i \leq M-1)$

$$\mathbf{D}_n\left(i,:\right) = \frac{\partial d_{G_{i+1},G_1 \to V_n}^*}{\partial \mathbf{v}_n} = \left[\mathbf{k}_{\mathbf{g}_{i+1}}^{\mathbf{v}_n^*} - \mathbf{k}_{\mathbf{g}_1}^{\mathbf{v}_n^*}\right]^T, \quad (35)$$

$$\mathbf{k}_{\mathbf{g}_m}^{\mathbf{v}_n^*} = \frac{\left(\mathbf{v}_n^* - \mathbf{g}_m\right)}{r_{G_m \to V_n}^*} = \frac{\left(\mathbf{v}_n^* - \mathbf{g}_m\right)}{\left\|\mathbf{v}_{n,3D}^* - \mathbf{g}_{m,3D}\right\|}. \quad (36)$$

Similarly, the partial derivative $\frac{\partial \mathbf{r}_{V\to V}^*}{\partial \mathbf{v}}$ of the DR-TWR measurements can be expressed as equations (37)-(39).

$$\frac{\partial \mathbf{r}_{V\to V}^*}{\partial \mathbf{v}} = \left[\mathbf{R}_1^T, \mathbf{R}_2^T, \cdots, \mathbf{R}_N^T\right]^T, \quad (37)$$

$$\mathbf{k}_{\mathbf{v}_{L_{n,i}}^*}^{\mathbf{v}_n^*} = \frac{\left(\mathbf{v}_n^* - \mathbf{v}_{L_{n,i}}^*\right)}{r_{V_n \to V_{L_{n,i}},i}^*} = \frac{\left(\mathbf{v}_n^* - \mathbf{v}_{L_{n,i}}^*\right)}{\left\|\mathbf{v}_{n,3D}^* - \mathbf{v}_{L_{n,i},3D}^*\right\|}. \quad (39)$$

We assume that the UAV self-localization performed at the GRS $G_1$ could approach the CRLB. Then, the covariance matrix of UAV position uncertainty can be approximated as

$$\mathbf{Q}_{\Delta\mathbf{v}} = \text{cov}\left(\Delta\mathbf{v}\right) = E\left[\left(\hat{\mathbf{v}} - \mathbf{v}^*\right)\left(\hat{\mathbf{v}} - \mathbf{v}^*\right)^T\right] \approx \text{CRLB}\left(\mathbf{v}\right), \quad (40)$$

where $\mathbf{v}^* = \left[\left(\mathbf{v}_1^*\right)^T, \cdots, \left(\mathbf{v}_N^*\right)^T\right]^T$, $\Delta\mathbf{v} = \left[\Delta\mathbf{v}_1^T, \cdots, \Delta\mathbf{v}_N^T\right]^T$.

### B. RMSE of UE Position Estimation

As described in Section II.C, the UE uses the ILS method to determine its own location. Since the position and clock uncertainty of UAVs are unknown, the UE can only use the following measurement equations for position estimation:

$$\bar{\mathbf{d}}_{V\to U}\left(\mathbf{u}\right) = \left[\bar{d}_{V_2, V_1 \to U}\left(\mathbf{u}\right), \cdots, \bar{d}_{V_N, V_1 \to U}\left(\mathbf{u}\right)\right]^T, \quad (41)$$

$$\bar{d}_{V_n, V_1 \to U}\left(\mathbf{u}\right) = \left\|\mathbf{u}_{3D} - \hat{\mathbf{v}}_{n,3D}\right\| - \left\|\mathbf{u}_{3D} - \hat{\mathbf{v}}_{1,3D}\right\|, \quad (42)$$

where $\mathbf{u}_{3D} = \left[\mathbf{u}^T, h_U\right]^T$.

The ILS method estimates the UE's location in an iterative manner through Taylor-series linearization [51]. Let $\hat{\mathbf{u}}_k = \left[\hat{x}_U^k, \hat{y}_U^k\right]^T$ ($\hat{\mathbf{u}}_{k,3D} = \left[\hat{\mathbf{u}}_k^T, h_U\right]^T$) denote the location estimate obtained in the $k$-th iteration, the first-order Taylor-series expansion of $\bar{\mathbf{d}}_{V\to U}\left(\mathbf{u}\right)$ at $\hat{\mathbf{u}}_k$ can be expressed as

$$\bar{\mathbf{d}}_{V\to U}\left(\mathbf{u}\right) \simeq \bar{\mathbf{d}}_{V\to U}\left(\hat{\mathbf{u}}_k\right) + \mathbf{H}\left(\hat{\mathbf{u}}_k\right)\left(\mathbf{u} - \hat{\mathbf{u}}_k\right), \quad (43)$$

where

$$\begin{aligned}\mathbf{H}\left(\hat{\mathbf{u}}_k\right) &= \left.\frac{\partial \bar{\mathbf{d}}_{V\to U}\left(\mathbf{u}\right)}{\partial \mathbf{u}}\right|_{\hat{\mathbf{u}}_k} \\ &= \left[\left(\mathbf{k}_{\hat{\mathbf{v}}_2}^{\hat{\mathbf{u}}_k} - \mathbf{k}_{\hat{\mathbf{v}}_1}^{\hat{\mathbf{u}}_k}\right), \cdots, \left(\mathbf{k}_{\hat{\mathbf{v}}_N}^{\hat{\mathbf{u}}_k} - \mathbf{k}_{\hat{\mathbf{v}}_1}^{\hat{\mathbf{u}}_k}\right)\right]^T \\ &\approx \left[\left(\mathbf{k}_{\mathbf{v}_2^*}^{\hat{\mathbf{u}}_k} - \mathbf{k}_{\mathbf{v}_1^*}^{\hat{\mathbf{u}}_k}\right), \cdots, \left(\mathbf{k}_{\mathbf{v}_N^*}^{\hat{\mathbf{u}}_k} - \mathbf{k}_{\mathbf{v}_1^*}^{\hat{\mathbf{u}}_k}\right)\right]^T,\end{aligned} \quad (44)$$

is the Jacobian matrix of measurement equations at $\hat{\mathbf{u}}_k$, and

$$\mathbf{k}_{\mathbf{v}_n^*}^{\hat{\mathbf{u}}_k} = \frac{\left(\hat{\mathbf{u}}_k - \mathbf{v}_n^*\right)}{\left\|\hat{\mathbf{u}}_{k,3D} - \mathbf{v}_{n,3D}^*\right\|}. \quad (45)$$

Noted that in equation (44), the estimated locations ($\hat{\mathbf{v}}_n$) of UAVs are replaced by the corresponding true values ($\mathbf{v}_n^*$). The explanation for this operation is explained in [43].

Then, the least-squares estimate of the UE's location obtained in the $(k+1)$-th iteration is given by

$$\begin{aligned}\hat{\mathbf{u}}_{k+1} = \hat{\mathbf{u}}_k + &\left(\mathbf{H}(\hat{\mathbf{u}}_k)^T \mathbf{Q}_{\mathbf{n}_{V\to U}}^{-1} \mathbf{H}\left(\hat{\mathbf{u}}_k\right)\right)^{-1} \mathbf{H}(\hat{\mathbf{u}}_k)^T \mathbf{Q}_{\mathbf{n}_{V\to U}}^{-1} \\ &\cdot \left(\mathbf{d}_{V\to U} - \bar{\mathbf{d}}_{V\to U}\left(\hat{\mathbf{u}}_k\right)\right).\end{aligned} \quad (46)$$

Replacing $\hat{\mathbf{u}}_k$ in the above equation with the UE's true location $\mathbf{u}^*$, the estimation error of the ILS method after convergence can be written as

$$\Delta\mathbf{u} = \hat{\mathbf{u}} - \mathbf{u}^* = \mathbf{S}\left(\mathbf{u}^*\right)\left(\mathbf{d}_{V\to U} - \bar{\mathbf{d}}_{V\to U}\left(\mathbf{u}^*\right)\right), \quad (47)$$

where

$$\mathbf{S}\left(\mathbf{u}^*\right) = \mathbf{P}\left(\mathbf{u}^*\right)\mathbf{H}(\mathbf{u}^*)^T \mathbf{Q}_{\mathbf{n}_{V\to U}}^{-1}, \quad (48)$$

$$\mathbf{P}\left(\mathbf{u}^*\right) = \left(\mathbf{H}(\mathbf{u}^*)^T \mathbf{Q}_{\mathbf{n}_{V\to U}}^{-1} \mathbf{H}\left(\mathbf{u}^*\right)\right)^{-1}; \quad (49)$$

$\mathbf{Q}_{\mathbf{n}_{V\to U}}$ denotes the covariance matrix of the noise term $\mathbf{n}_{V\to U}$ in equation (21), and can be expressed as

$$\mathbf{Q}_{\mathbf{n}_{V\to U}} = \sigma_{V_1 \to U}^2 \cdot \mathbf{I}_{N-1} + \text{diag}\left(\sigma_{V_2 \to U}^2, \cdots, \sigma_{V_N \to U}^2\right). \quad (50)$$

We then derive the expression for term $\left(\mathbf{d}_{V\to U} - \bar{\mathbf{d}}_{V\to U}\left(\mathbf{u}^*\right)\right)$ in equation (47). The difference between the measured TDoA $d_{V_n, V_1 \to U}$ and the TDoA value $\bar{d}_{V_n, V_1 \to U}\left(\mathbf{u}^*\right)$ that is predicted from equation (42) can be written as

$$\begin{aligned}d_{V_n, V_1 \to U} - \bar{d}_{V_n, V_1 \to U}\left(\mathbf{u}^*\right) = &\left(d_{V_n, V_1 \to U}^* - \Delta t_{V_n, V_1 \to U}^{Pos}\right. \\ &\left. - \Delta t_{V_n, V_1 \to U}^{Noi} + n_{V_n, V_1 \to U}\right) \\ &- \left(\left\|\mathbf{u}_{3D}^* - \hat{\mathbf{v}}_{n,3D}\right\| - \left\|\mathbf{u}_{3D}^* - \hat{\mathbf{v}}_{1,3D}\right\|\right),\end{aligned} \quad (51)$$

where the expression of $\Delta t_{V_n, V_1 \to U}^{Pos}$ is

$$\begin{aligned}\Delta t_{V_n, V_1 \to U}^{Pos} = &\left(\left\|\hat{\mathbf{v}}_{n,3D} - \mathbf{g}_{1,3D}\right\| - \left\|\mathbf{v}_{n,3D}^* - \mathbf{g}_{1,3D}\right\|\right) \\ &- \left(\left\|\hat{\mathbf{v}}_{1,3D} - \mathbf{g}_{1,3D}\right\| - \left\|\mathbf{v}_{1,3D}^* - \mathbf{g}_{1,3D}\right\|\right).\end{aligned} \quad (52)$$

Expanding the term $\|\hat{\mathbf{v}}_{n,3D} - \mathbf{g}_{1,3D}\|$ at $\mathbf{v}_{n,3D}^*$ based on the relationship $\hat{\mathbf{v}}_{n,3D} = \mathbf{v}_{n,3D}^* + [\Delta\mathbf{v}_n^T, 0]^T$, we have

$$\|\hat{\mathbf{v}}_{n,3D} - \mathbf{g}_{1,3D}\| \simeq \|\mathbf{v}_{n,3D}^* - \mathbf{g}_{1,3D}\| + \left(\mathbf{k}_{\mathbf{g}_1}^{\mathbf{v}_n^*}\right)^T \Delta\mathbf{v}_n. \quad (53)$$

Thus, $\Delta t_{V_n, V_1 \to U}^{Pos}$ in equation (51) can be approximated as

$$\Delta t_{V_n, V_1 \to U}^{Pos} \approx \left(k_{\mathbf{g}_1}^{\mathbf{v}_n^*}\right)^T \Delta\mathbf{v}_n - \left(k_{\mathbf{g}_1}^{\mathbf{v}_1^*}\right)^T \Delta\mathbf{v}_1. \quad (54)$$

Similarly, the term $\|\mathbf{u}_{3D}^* - \hat{\mathbf{v}}_{n,3D}\|$ in equation (51) can be expanded as

$$\|\mathbf{u}_{3D}^* - \hat{\mathbf{v}}_{n,3D}\| \simeq \|\mathbf{u}_{3D}^* - \mathbf{v}_{n,3D}^*\| - \left(\mathbf{k}_{\mathbf{v}_n^*}^{\mathbf{u}^*}\right)^T \Delta\mathbf{v}_n, \quad (54)$$

and $\bar{d}_{V_n, V_1 \to U}(\mathbf{u}^*)$ can be approximated as

$$\begin{aligned}
\bar{d}_{V_n, V_1 \to U}(\mathbf{u}^*) &\approx \left(\|\mathbf{u}_{3D}^* - \mathbf{v}_{n,3D}^*\| - \left(\mathbf{k}_{\mathbf{v}_n^*}^{\mathbf{u}^*}\right)^T \Delta\mathbf{v}_n\right) \\
&\quad - \left(\|\mathbf{u}_{3D}^* - \mathbf{v}_{1,3D}^*\| - \left(\mathbf{k}_{\mathbf{v}_1^*}^{\mathbf{u}^*}\right)^T \Delta\mathbf{v}_1\right) \\
&= d_{V_n, V_1 \to U}^* - \left(\mathbf{k}_{\mathbf{v}_n^*}^{\mathbf{u}^*}\right)^T \Delta\mathbf{v}_n + \left(\mathbf{k}_{\mathbf{v}_1^*}^{\mathbf{u}^*}\right)^T \Delta\mathbf{v}_1.
\end{aligned} \quad (55)$$

Then, the expression of $d_{V_n, V_1 \to U} - \bar{d}_{V_n, V_1 \to U}(\mathbf{u}^*)$ can be written as

$$\begin{aligned}
d_{V_n, V_1 \to U} - \bar{d}_{V_n, V_1 \to U}(\mathbf{u}^*) &= \left(\mathbf{k}_{\mathbf{v}_n^*}^{\mathbf{u}^*} - \mathbf{k}_{\mathbf{g}_1}^{\mathbf{v}_n^*}\right)^T \Delta\mathbf{v}_n \\
&\quad - \left(\mathbf{k}_{\mathbf{v}_1^*}^{\mathbf{u}^*} - \mathbf{k}_{\mathbf{g}_1}^{\mathbf{v}_1^*}\right)^T \Delta\mathbf{v}_1 - \Delta t_{V_n, V_1 \to U}^{Noi} + n_{V_n, V_1 \to U}.
\end{aligned} \quad (56)$$

Therefore, the term $\left(\mathbf{d}_{V \to U} - \bar{\mathbf{d}}_{V \to U}(\mathbf{u}^*)\right)$ in equation (47) can be expressed as

$$\mathbf{d}_{V \to U} - \bar{\mathbf{d}}_{V \to U}(\mathbf{u}^*) = \mathbf{K}_{V \to U}\Delta\mathbf{v} - \Delta\mathbf{t}_{V \to U}^{Noi} + \mathbf{n}_{V \to U}, \quad (57)$$

where $\mathbf{K}_{V \to U}$ is a $(N-1) \times 2N$ matrix and its expression can be written as $(1 \le i \le N-1)$

$$\begin{aligned}
\mathbf{K}_{V \to U}(i,:) = \Big[ &-\left(\mathbf{k}_{\mathbf{v}_1^*}^{\mathbf{u}^*} - \mathbf{k}_{\mathbf{g}_1}^{\mathbf{v}_1^*}\right)^T, \mathbf{0}_{2(i-1)\times 1}^T, \\
&\left(\mathbf{k}_{\mathbf{v}_{i+1}^*}^{\mathbf{u}^*} - \mathbf{k}_{\mathbf{g}_1}^{\mathbf{v}_{i+1}^*}\right)^T, \mathbf{0}_{2(N-i-1)\times 1}^T \Big].
\end{aligned} \quad (58)$$

With equations (47) and (57), the covariance matrix of the UE position error is derived as

$$\begin{aligned}
\mathbf{Q}_{\Delta\mathbf{u}} &= \mathrm{cov}(\Delta\mathbf{u}) = E\left[(\hat{\mathbf{u}} - \mathbf{u}^*)(\hat{\mathbf{u}} - \mathbf{u}^*)^T\right] \\
&= E\Big[\mathbf{S}(\mathbf{u}^*)\left(\mathbf{K}_{V \to U}\Delta\mathbf{v} - \Delta\mathbf{t}_{V \to U}^{Noi} + \mathbf{n}_{V \to U}\right) \\
&\quad \left(\mathbf{K}_{V \to U}\Delta\mathbf{v} - \Delta\mathbf{t}_{V \to U}^{Noi} + \mathbf{n}_{V \to U}\right)^T \mathbf{S}(\mathbf{u}^*)^T\Big] \\
&= \mathbf{P}(\mathbf{u}^*) + \mathbf{S}(\mathbf{u}^*)\left(\mathbf{K}_{V \to U}\mathbf{Q}_{\Delta\mathbf{v}}\mathbf{K}_{V \to U}^T + \mathbf{Q}_{\Delta\mathbf{t}_{V \to U}^{Noi}}\right)\mathbf{S}(\mathbf{u}^*)^T,
\end{aligned} \quad (59)$$

where

$$\mathbf{Q}_{\Delta\mathbf{t}_{V \to U}^{Noi}} = \sigma_{G_1 \to V_1}^2 \cdot \mathbf{I}_{N-1} + \mathrm{diag}\left(\sigma_{G_1 \to V_2}^2, \cdots, \sigma_{G_1 \to V_N}^2\right). \quad (60)$$

Finally, the RMSE of UE position estimate can be calculated as follows:

$$\mathrm{RMSE}(\mathbf{u}) = \mathrm{trace}(\mathbf{Q}_{\Delta\mathbf{u}})^{\frac{1}{2}}. \quad (61)$$

As can be seen from equation (59), the covariance matrix $\mathbf{Q}_{\Delta\mathbf{u}}$ is the sum of two terms. The first term

$(\mathbf{P}(\mathbf{u}^*))$ represents the UE position error under ideal conditions where UAVs' locations are perfectly known and their clocks are accurately synchronized. The second term $(\mathbf{S}(\mathbf{u}^*)\left(\mathbf{K}_{V \to U}\mathbf{Q}_{\Delta\mathbf{v}}\mathbf{K}_{V \to U}^T + \mathbf{Q}_{\Delta\mathbf{t}_{V \to U}^{Noi}}\right)\mathbf{S}(\mathbf{u}^*)^T)$ reflects the impacts of UAV position uncertainty and synchronization errors caused by noise and jamming on position accuracy.

### C. Other Performance Metrics

With the expressions derived in the above two subsections, we can quantitatively evaluate the accuracy of the UAV self-localization and UE position estimation in jamming environments. Although the position accuracy is the major concern in this article, it is still not sufficient to comprehensively evaluate the quality of positioning services. In order to demonstrate the feasibility and practicability of the proposed system in real-world applications, it is necessary to evaluate and analyze some other performance metrics of the positioning service. Thus, in this subsection, we discuss three metrics other than the position accuracy, that is, energy consumption, time delay and computational complexity.

In the proposed system, the UEs' energy consumption is negligible, because they only need to receive positioning signals and estimate their own locations. Moreover, GRSs commonly have the ability to carry enough batteries to support long-term missions and their energy can be easily replenished in many ways. On the contrary, UAVs not only need to transmit signals for self-localization and positioning services, but also have very limited on-board energy due to size and weight constraints. Thus, the UAVs' energy consumption is the main factor affecting the continuity of positioning services. The energy consumption of UAVs consists of three parts, namely the signal transmission energy, the energy for signal reception and processing, as well as the hovering energy required for keeping UAVs at the pre-determined locations. Since previous research has widely accepted the view that the energy consumption for signal reception is much lower than for transmission [52], we will simply ignore this energy consumption in the following analysis. Assuming that the UAV self-localization has the same period as the positioning service, in each positioning period, each UAV needs to transmit $(N-1)$ request messages and $2(N-1)$ response messages through V2V links for self-localization. Moreover, a frame of positioning signal needs to be broadcast through the V2U link to support the TDoA positioning service. We also assume that the transmission of a request/response message requires the same amount of energy as the broadcast of a signal frame for the positioning service. Then, for each UAV, its transmission energy consumption in jamming environments is $(3N-2)$ times larger than that in normal environments where the self-localization can be performed with the on-board GNSS receiver. So it seems that the operation of UAVs in the proposed system requires high energy consumption. In fact, as many existing research pointed out, the energy consumption of a UAV is actually dominated by its hovering energy [53], [54]. In addition, as will be introduced in Section IV.E, the transmission energy consumption can be controlled within an acceptable range by selecting energy-efficient transmit power

for UAVs. Therefore, in practical applications, the UAVs' energy consumption will not be a major issue threatening the proposed system's practicability.

Time delay is a metric to measure the real-time performance of positioning services, and its value is very important for user experience. As introduced in the previous section, the operation of the proposed system includes two processes, namely the UAV self-localization process and the service process. During the self-localization process, the GRSs first simultaneously broadcast positioning signals through G2V links to provide TDOA measurements for UAVs. Since GRSs use pseudo-random sequences with good cross-correlation properties, the interference among positioning signals is negligible compared to jamming. The frame length of positioning signals broadcast by GRSs is denoted by $\tau_S$. Then, UAVs utilize the V2V links to perform DR-TWR measurement in pairs. For now, the DR-TWR measurements corresponding to different UAV pairs need to be performed in different time slots. Thus, $N(N-1)$ time slots are required to complete the DR-TWR measurement in the proposed system. As described in Appendix A, the length of a time slot for DR-TWR measurement can be approximated as $2\tau_D$. Then, the time delay caused by the UAV self-localization process is $2N(N-1)\tau_D + \tau_S$. After their time and locations are determined, all UAVs broadcast positioning signals with frame length of $\tau_S$ at the same time to provide TDoA positioning services for UEs. Thus, in the proposed system, the total time delay between UE's request and service provision is $2N(N-1)\tau_D + 2\tau_S$. It is noteworthy that the total time delay of positioning services may be very large as the number of UAVs increases. However, as will be introduced in section IV, numerical results show that only six UAVs are needed to provide positioning services with accuracy better than 20m for UEs in target area with size of $500\text{m} \times 500\text{m}$. Therefore, in practical applications, the time delay of the proposed system is acceptable. Moreover, the time delay can be reduced by adopting more flexible DR-TWR protocol that allows multiple DR-TWR measurements to be performed simultaneously, which will be studied in our future work.

In terms of the computational complexity, the UAVs' locations are estimated with the well-known ML method. In practical applications, the maximum likelihood estimates can be obtained with iterative algorithms like Gauss-Newton (GN) method through a number of iterations [55]. As described at the end of Section II.A, the total number of measurements used to estimate the UAVs' locations is $N \times (M+N-2)$. Then, in each iteration of the GN method, the Newton step can be calculated with complexity of $\mathcal{O}\left(N^3(N+M-2)^3\right)$. If the number of iterations required for the GN method to converge is $K_{ML}$, the total computational complexity of maximum likelihood estimation for UAV self-localization can be expressed as $\mathcal{O}\left(K_{ML}N^3(N+M-2)^3\right) \approx \mathcal{O}\left(K_{ML}N^3(N+M)^3\right)$. Obviously, the implementation of the ML method is computationally intensive and time-consuming, especially when the numbers of UAVs and GRSs are very large. Therefore, in the proposed system, we choose the GRS to perform UAV location estimation. Since the GRS can carry equipment

TABLE I
SIMULATION PARAMETERS

| Parameter | Value |
|---|---|
| Main frequency ($f_c$) | 2.4 GHz |
| Signal bandwidth ($B$) | 10 MHz |
| Noise power ($P_{n_0}$) | -95 dBm |
| Reference path loss at 1m ($\beta_0$) | $1.01 \times 10^4$ |
| PLE of G2A channels under LoS conditions ($\alpha_{G2A}^L$) | 2 |
| PLE of G2A channels under NLoS conditions ($\alpha_{G2A}^N$) | 3.2 |
| PLE of G2G channels under LoS conditions ($\alpha_{G2G}^L$) | 2.2 |
| PLE of G2G channels under NLoS conditions ($\alpha_{G2G}^N$) | 3.5 |
| Height of the jammer's antenna ($h_J$) | 5 m |
| Transmit power of the jammer ($P_J^t$) | 20 dBm |
| Radius of the jamming area ($R_J$) | 2.5 km |
| Number of GRSs ($M$) | 6 |
| Height of GRSs' antenna ($h_G$) | 25 m |
| Transmit power of GRSs ($P_G^t$) | 35 dBm |
| Number of UAV ($N$) | 6 |
| UAV altitude ($h_V$) | 100 m |
| Transmit power of UAVs ($P_V^t$) | 30 dBm |
| Height of the UE's antenna ($h_U$) | 1.5 m |
| Side length of the target area ($L_T$) | 500 m |

with sufficient computation power, the complexity of the ML method is actually acceptable. In addition, the problem of high computational complexity can be solved by replacing the ML method with some low-complexity methods. Since the development of novel estimation methods goes beyond the scope of this article, we will study this issue in our future work. In terms of the ILS method for UE location estimation, it has already been used by GNSS receivers and cell phones for decades. Therefore, the implementation of the ILS method is an easy task for users' handheld devices, so its computational complexity is not analyzed in this article. Based on the above analysis, we believe that the computational complexity of location estimation methods will not threaten the proposed system's practicability in real-world applications.

## IV. NUMERICAL RESULTS

In this section, a series of simulation experiments are conducted to evaluate the performance of the proposed system under jamming attacks, and the corresponding numerical results are presented to verify its feasibility and validity. First, we test and compare the position accuracy of the proposed UAV-assisted system and the conventional terrestrial positioning system using only GRSs in a typical jamming scenario. Then, the key factors affecting the anti-jamming performance of our system and their influence on position accuracy are analyzed in detail through several experiments. Table I summarizes the key simulation parameters used in this section.

Fig. 4 shows the jamming scenario for performance evaluation in this section, which consists of 6 GRSs, 6 UAVs and a jammer. The location of the jammer is set as the
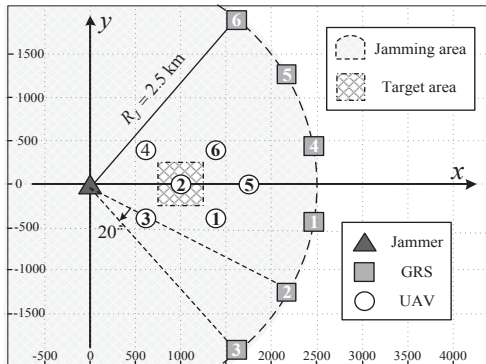
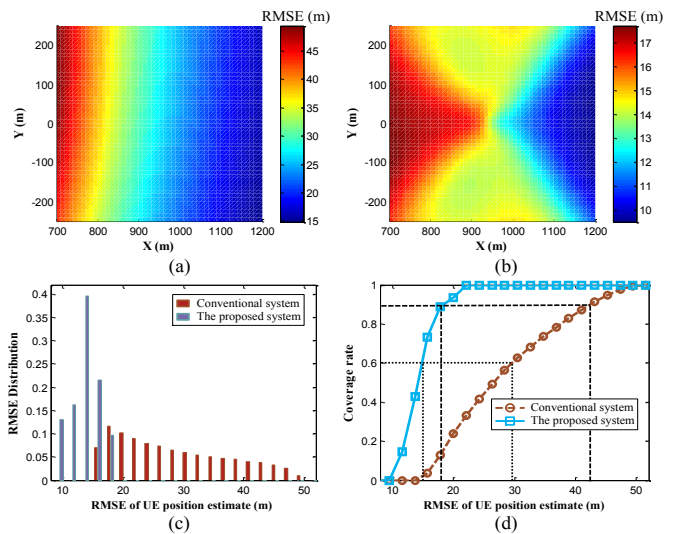Fig. 4. Typical jamming scenario for numerical evaluation.



Fig. 5. Feasibility and performance of the proposed system: (a) UE position RMSE of the conventional (G2U LoS links exist) and (b) the proposed systems, (c) RMSE distributions and (d) service coverage of the two systems.

origin of coordinates, that is, $\mathbf{w} = [0,0]^T$. GRSs are located on the boundary of the jamming area, and the difference between the azimuth angles of two adjacent GRSs is 20 degree. The horizontal coordinates of the 6 UAVs are set to $\mathbf{v}_1^* = [1350, -400]^T$, $\mathbf{v}_2^* = [950, 0]^T$, $\mathbf{v}_3^* = [550, -400]^T$, $\mathbf{v}_4^* = [550, 400]^T$, $\mathbf{v}_5^* = [1750, 0]^T$ and $\mathbf{v}_6^* = [1350, 400]^T$. The J2V links between UAVs and the jammer are dominated by LoS components. The target area where UEs are located is a square with center at $\mathbf{o}_T = [950, 0]^T$ and side length of 500m. During the simulation, the target area will be discretized into a series of sample points with an interval of 10m, and the position accuracy at each sample point would be calculated and recorded for performance evaluation.

### A. Feasibility and Validity of the Proposed System

With the expressions derived in Section III, we calculate the theoretical RMSE of UE position estimate of the proposed system in the jamming scenario mentioned above, and compare it with the conventional terrestrial system using only GRSs. For the conventional system, we assume that there are LoS paths between GRSs and UEs. The evaluation results of the two systems are shown in Fig. 5. Comparing the "heat maps" shown in Fig. 5(a) and (b), it can be found that the maximum RMSE of the proposed system in the target area is 17.7m, which is 64.2% lower than the value of 49.4m for the conventional system.

Moreover, in Fig. 5(c) and (d), we further analyze the RMSE distribution and service coverage rate of the two systems in the target area. As can be seen from Fig. 5(c), the conventional system's RMSE at most sample points is between 20m and 50m, much larger than the maximum RMSE of the proposed system. Only at a few locations is the RMSE of the conventional system less than 20m, which is comparable to the proposed system's performance. The "service coverage rate" in Fig. 5(d) reflects the proportion of the areas with RMSE less than a certain value in the entire target area. For example, the conventional system's RMSE corresponding to the 90% coverage rate is 42.5m, which can be interpreted as: when using the conventional system, the positioning service with RMSE less than 42.5m could cover 90% of the target area. As can be seen from Fig. 5(d), the proposed system's 60% and 90% coverage RMSE is 14.9m and 18.5m, much smaller than

the values of 29.7m and 42.5m for the conventional system. Therefore, it can be concluded from the above analysis that in jamming environments, the proposed UAV-assisted system outperforms the conventional terrestrial system in terms of maximum RMSE, RMSE distribution and service coverage, which demonstrate the feasibility and validity of our system.

The above evaluation results are quite reasonable. Due to the existence of the jamming area, the geometry of GRSs is not favourable for the positioning service, resulting in poor accuracy for the conventional terrestrial system. Thus, although their position and clock uncertainty will introduce additional errors in UE location estimation, UAVs with satisfactory geometry could still achieve better performance than the conventional system. Noted that this simulation experiment is based on the assumption that the propagation condition of G2U links is LoS, which may not be true in practice due to the long distance between GRSs and UEs. When there is no LoS path in G2U links, the conventional system cannot provide positioning services, while the proposed system can still work efficiently, which also reflects the superiority of our system.

### B. The Importance of V2V Links in the Proposed System

As described in Section II.A, UAVs in the proposed system utilize the TDoA measurements from G2V links and the DR-TWR measurements from V2V links to determine their own locations. Obviously, the G2V link is indispensable for UAV self-localization as it provides valuable information about the UAVs' absolute locations. In contrast, the role of the V2V measurement link in the proposed system is less clear. Thus, in this subsection, we carry out a simulation experiment to verify the importance of the V2V links.

We first generate a simplified version of the proposed system by removing all V2V links, and then calculate its theoretical performance in the target area. The CRLB of the UAV self-localization without V2V links can be obtained by excluding the term $\mathbf{J}_{V \to V}^{DR-TWR}$ in equation (33). Assigning the newly
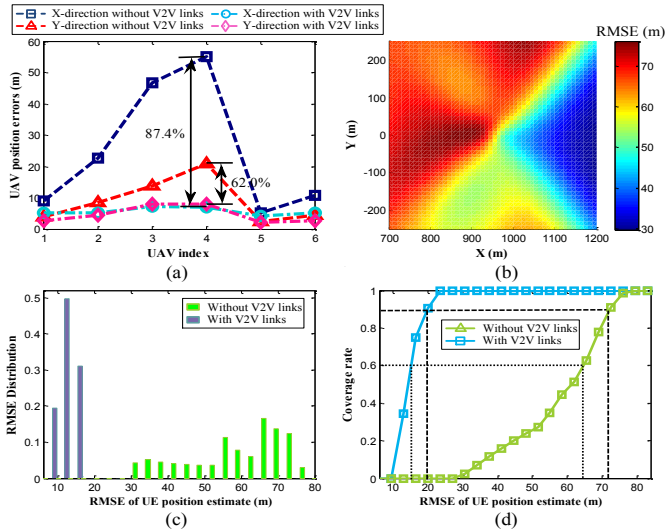
Fig. 6. Importance of V2V links: (a) UAV position errors under two conditions (with or without V2V links), (b) UE position RMSE without V2V links, (c) RMSE distributions and (d) service coverage under two conditions.
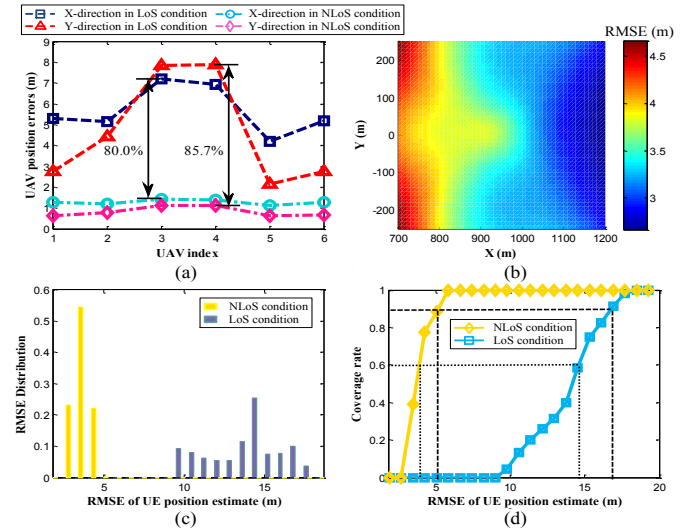


Fig. 7. Influence of NLoS propagation in J2V links: (a) UAV position errors under two conditions (J2V NLoS or LoS), (b) UE position RMSE when the propagation condition of J2V links is NLoS, (c) RMSE distribution and (d) service coverage under two conditions.

calculated CRLB to the matrix $\mathbf{Q}_{\Delta \mathbf{v}}$ in equation (59), then the expressions derived in Section III.B can also be used to calculate the RMSE of UE position estimate in the simplified system. The performance evaluation results for this case are shown in Fig. 6.

It can be seen from Fig. 6(a) that the existence of V2V links reduces the maximum UAV position error in the x- and y-directions by 87.4% and 62.0%, respectively. Intuitively, the reason for the huge improvement in the UAV position accuracy is that V2V links greatly reduce the impact of the GRSs' geometry on UAV self-localization. In the absence of V2V links, most of the GRSs are located on the right side of UAVs (Fig. 4), resulting in poor geometry of anchor nodes, especially in the x-direction. With the V2V links, each UAV could be regarded as an anchor node for other UAVs, which improves the geometry and leads to satisfactory performance of UAV self-localization. As shown in Fig. 6(b), the maximum RMSE of the simplified system in the target area is 76.1m, about four times larger than the value of 17.7m for the proposed system (Fig. 5(b)) and even worse than that of the conventional terrestrial system (Fig. 5(a)). Moreover, it can be seen from Fig. 6(c) that the RMSE of the proposed system at all sample points is much smaller than the minimum RMSE of the simplified system without V2V links. Since the V2V links greatly reduce the UAV position uncertainty, it is natural that the UE position accuracy would be improved. In addition, according to Fig. 6(d), the simplified system's 60% and 90% coverage RMSE is 64.7m and 72.3m, which is significantly worse than that of the proposed system. All of these findings demonstrate the importance of V2V links in the proposed UAV-assisted system.

### C. The Influence of J2V Links' Propagation Conditions

Unlike UEs, UAVs with high maneuverability are capable of changing the propagation conditions of J2V links through strategies like hiding behind buildings or mountains, so as to

mitigate the impact of jamming on positioning services. In order to investigate the influence of J2V links' propagation conditions on the proposed system's performance, we change the condition to NLoS and repeat the performance evaluation. The evaluation results are shown in Fig. 7.

It can be seen from Fig. 7(a) that in terms of UAV self-localization, changing the condition from LoS to NLoS reduces the maximum position error in x- and y-directions by 80.0% and 85.7%, respectively. Since the change of the propagation condition greatly weakens the power of jamming signals received at UAVs, the reduction of UAV position error is not surprising. According to Fig. 7(b) and (c), the RMSE of UE position estimate in the entire target area under NLoS conditions is less than 4.7m, which is only about half of the minimum RMSE obtained under LoS conditions. Moreover, the curves in Fig. 7(d) show that the 60% and 90% coverage RMSE of the proposed system under NLoS conditions is 3.9m and 5.1m, which meets the requirements of meter-level positioning services.

The evaluation results in this subsection demonstrate that the NLoS propagation in J2V links is beneficial for improving the position accuracy of both the UAV and UE. Therefore, in practical applications, as long as the positioning services are not affected, UAVs should flexibly adjust their locations to avoid LoS paths between them and the jammer.

### D. The Influence of GRSs' Signal-to-Jammer Ratio

In this subsection, a simulation experiment is conducted to investigate the influence of GRSs' signal-to-jammer transmit power ratio (SJR) on the proposed system's performance. During the experiment, the transmit power of UAVs and the jammer is set according to Table I and remains unchanged, while the GRSs' power increases from 25 to 45dBm (SJR: 5 to 25dB). We evaluate the performance of the proposed system, its simplified version without V2V links, and the conventional
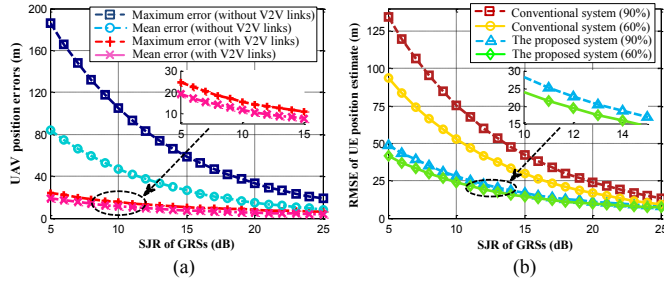
Fig. 8. Influence of GRSs' Signal-to-Jammer Transmit Power Ratio (SJR) on (a) UAV and (b) UE positioning performance.
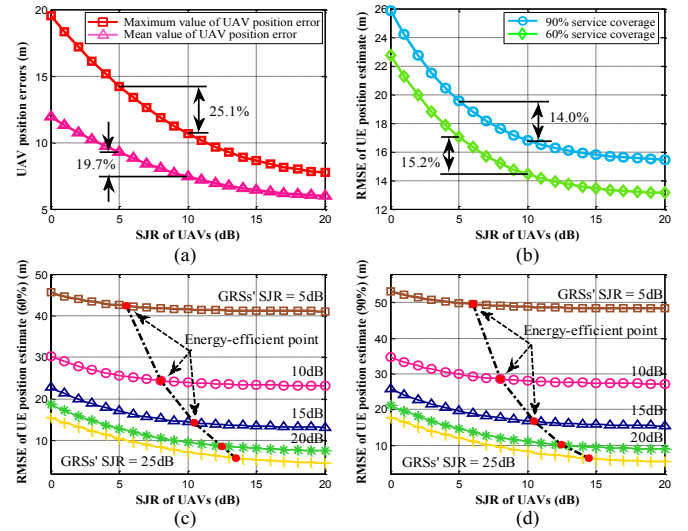


Fig. 9. Influence of UAVs' Signal-to-Jammer Transmit Power Ratio (SJR) on (a) UAV and (b) UE positioning performance, energy-efficient points for (c) 60% and (d) 90% service coverage.

terrestrial system at each SJR. Both the CRLB of UAV self-localization and RMSE of UE position estimate are calculated. The simulation results obtained are shown in Fig. 8.

It can be seen that the position accuracy of both the UAV and UE improves with the increase of the GRSs' SJR. As shown in Fig. 8(a), in terms of UAV self-localization, increasing the SJR from 5 to 10dB reduces the maximum and mean UAV position errors in the proposed system by 37.4% and 39.6%, respectively. Moreover, as the GRSs' SJR exceeds 20dB, the UAV position accuracy of the simplified system becomes very close to that of the proposed system. The explanation for this phenomenon is that the SINR of the V2V links does not change with GRSs' transmit power, so that the location information provided by V2V links is negligible when GRSs' SJR is extremely high.

According to Fig. 8(b), in terms of the positioning services provided for UE, as the SJR increases from 5 to 10dB, the 60% and 90% coverage RMSE of the proposed system is reduced by 42.4% and 42.5%, respectively. Under the condition of SJR > 20dB, the RMSE of the conventional system is close to that of the proposed system. The reason for this phenomenon is quite similar to that explained in the previous paragraph, that is, due to their constant transmit power, UAVs no longer have advantages in anti-jamming after the GRSs' SJR exceeds a certain value. Of course, if there is no LoS path between GRSs and UEs, UAVs would always be the best choice to provide positioning services for the target area regardless of the GRSs' SJR. In addition, it can be found in Fig. 8(b) that the reduction in the proposed system's RMSE slows down with the increase of SJR. This is because the UE position error caused by the noise and jamming in V2U links does not change with GRSs' SJR. If GRSs further increase their transmit power, the second term of equation (59) will approach 0, and the RMSE of the proposed system could be approximately calculated with the first term $\mathbf{P}(\mathbf{u}^*)$, indicating that the impact of UAV position and clock uncertainty on UE position accuracy is negligible.

### E. The Influence of UAVs' Signal-to-Jammer Ratio

Unlike GRSs, UAVs with size and weight constraints commonly have very limited on-board energy, so their transmit power should be chosen carefully. In this subsection, we analyze the influence of UAVs' SJR on the proposed system's performance and try to find the transmit power that provides the best balance of position accuracy and energy efficiency.

During the simulation, the transmit power of GRSs and the jammer remains constant as shown in Table I, while the UAVs' power varies from 20 to 40dBm (SJR: 0 to 20dB). The performance of the proposed system at each SJR is evaluated and shown in Fig. 9.

It can be seen from Fig. 9(a) and (b) that increasing the SJR of UAVs could significantly improve the performance of the UAV self-localization and UE positioning. According to Fig. 9(a), when the SJR increased from 5 to 10dB, the maximum and mean UAV position errors in the proposed system were reduced by 25.1% and 19.7%, respectively. The 60% and 90% coverage RMSE of the UE position estimate was reduced by 15.2% and 14.0%, as shown in Fig. 9(b). Moreover, it is noteworthy that the reductions in the UAV and UE position errors slow down as the SJR increases. The explanation for this phenomenon is that the SINR of G2V links that provide absolute location information for UAVs does not change with the UAVs' SJR. Thus, there is an upper limit to the improvement of the UAV and UE position accuracy brought about by the increase of SJR. It is unwise to continue to increase the UAVs' transmit power while the power of GRSs remains unchanged.

In order to avoid unnecessary wastage of on-board energy, we try to find the energy-efficient transmit power for UAVs in the proposed system. The curves in Fig. 9(c) and (d) show the RMSE of UE position estimate obtained at different GRSs' SJR and UAVs' SJR. Our approach for power selection is as follows: gradually increase the UAVs' power from 20dBm. If the RMSE reduction caused by a further increase of 0.5dBm in power is less than 0.15m, then the current power is regarded as an energy-efficient transmit power level for UAVs. The UAVs' SJR corresponding to the transmit power selected by this approach is indicated by the red dots in Fig. 9(c) and (d). For example, when the SJR of GRSs is 20dB, the UAVs' energy-efficient power for 60% service coverage is 30.5dBm (SJR: 10.5dB). The energy-efficient transmit power for 60%
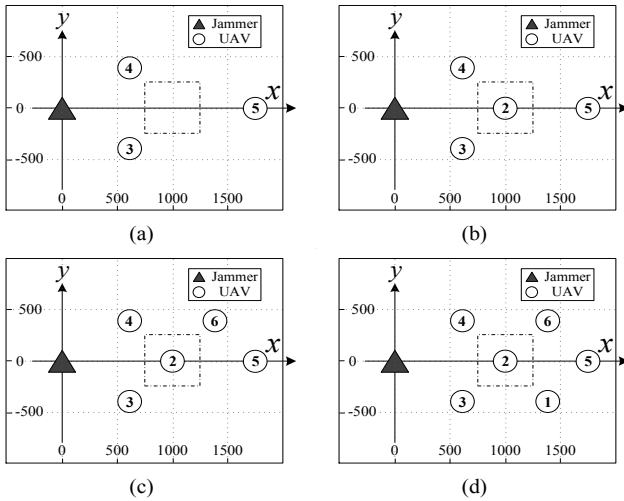
Fig. 10. Influence of the number of UAVs on system performance: Scenarios for (a) 3 UAVs, (b) 4 UAVs, (c) 5 UAVs and (d) 6 UAVs.
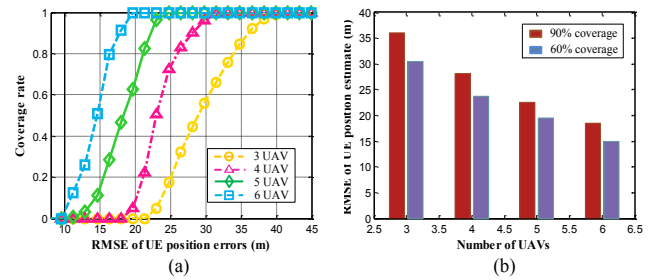


Fig. 11. Influence of the number of UAVs on system performance: (a) Service coverage and (b) 60%(90%) coverage RMSE corresponding to different numbers of UAVs.

and 90% service coverage is slightly different (no more than 1dBm), and can be selected according to mission requirements in practice.

### F. The Influence of the Number of UAVs

In the proposed system, after the self-localization and synchronization process, UAVs with known locations and synchronized clocks will be employed as aerial anchor nodes to provide TDoA positioning services for ground users. Obviously, the number of anchor nodes is one of the key factors affecting the quality of positioning services. Therefore, in this subsection, a series of simulation experiments are carried out to investigate the influence of the number of UAVs on the proposed system's performance.

As shown in Fig. 10(a) to (d), we construct four scenarios with different numbers of UAVs by removing certain UAVs from the typical jamming scenario shown in Fig. 4. Specifically, we remove UAV 1, 2 and 6 to construct a scenario with three UAVs as shown in Fig. 10(a); The four UAV scenario shown in Fig. 10(b) is constructed by adding UAV 2 to the above three UAV scenario; In terms of the five UAV scenario, only UAV 1 is removed, as shown in Fig. 10(c); Finally, the six UAV scenario shown in Fig. 10(d) is exactly the typical jamming scenario used in the previous subsections. Please note that the number of UAVs used in the proposed system should not be less than three, which is the minimum number of anchor nodes required for two-dimensional (2-D) TDoA positioning. To analyze the influence of the number of UAVs on positioning services, we successively apply the proposed system to the four scenarios mentioned above, and utilize the expressions derived in Section III to evaluate its performance in different scenario. During the simulation, the values of parameters other than the number of UAVs are set according to Table I and remain unchanged. The performance evaluation results obtained are shown in Fig. 11.

It can be seen from Fig. 11(a) that the service coverage of the proposed system improves significantly with the increase

of the number of UAVs. Accordingly, the 60% and 90% coverage RMSE in the target area decreases as the number of UAVs increases, as shown in Fig. 11(b). Numerically speaking, the 60% and 90% coverage RMSE obtained in the five UAV scenario (green solid line in Fig. 11(a)) is 19.4m and 22.6m, which is only about 36.4% and 37.4% of the 30.5m and 36.1m obtained in the three UAV scenario (yellow dash line). Moreover, the average reduction of the 60% and 90% coverage RMSE brought about by adding one UAV is about 21.2% and 22.1%, respectively. These phenomena indicate that increasing the number of UAVs used in the proposed system is conducive to the improvement of positioning performance. In general, six UAVs are needed to achieve a position accuracy better than 20m. However, it is also observed that the reduction in the proposed system's RMSE slows down as the number of UAVs increases. When there are only three UAVs in the proposed system, increasing the number of UAVs to four could reduce the 90% coverage RMSE by 22.1%. If the current number of UAVs is 5, the reduction of the 90% coverage RMSE brought about by adding one UAV is only 18.1%. Therefore, in practical applications, we should not always try to improve the position accuracy by adding more UAVs, especially when other factors like safety and cost are taken into consideration.

### G. The Influence of UAV Deployment Strategy

In addition to the number of anchors nodes, the geometry of anchor nodes relative to the user is also a key factor that could strongly affect the positioning accuracy of a positioning system. As discussed in subsection A, one of the reasons for the poor performance of the conventional system is that the geometry of GRSs is not favorable for the positioning service. Moreover, the main advantage of the UAVs that are used as aerial anchor nodes in this article is their fully controllable mobility and flexible deployment. Thus, in order to improve the practicability of the proposed system, it is necessary to study the influence of UAV deployment on system performance. Then, in this subsection, several simulation experiments are conducted to show how the selection of UAVs' locations affects the position accuracy.

Similar to the operations performed in the previous subsection, we first construct four scenarios corresponding to different UAV deployment strategies by removing one UAV from the typical jamming scenario, as shown in Fig. 12(a) to (d). Specifically, as shown in Fig. 12(a), we remove UAV
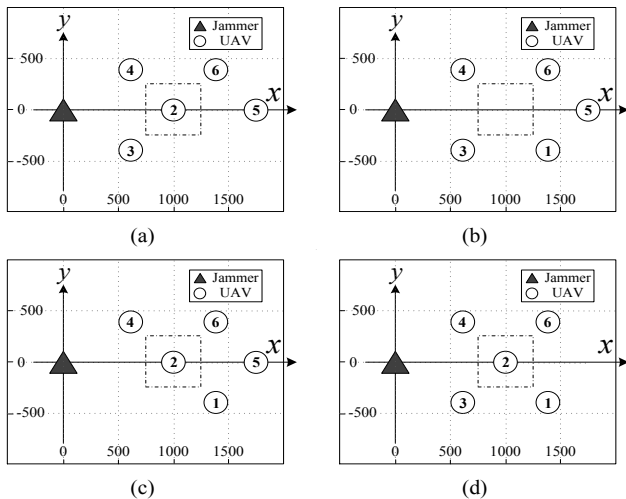
Fig. 12. Influence of the UAV deployment strategy on system performance: Scenarios for deployment (a) strategy 1, (b) strategy 2, (c) strategy 3 and (d) strategy 4.
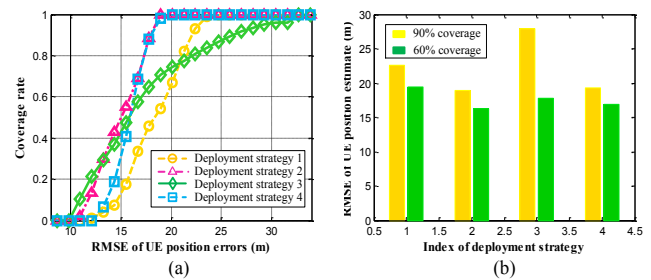


Fig. 13. Influence of the UAV deployment strategy on system performance: (a) Service coverage and (b) 60%(90%) coverage RMSE corresponding to different UAV deployment strategies.

1 to form deployment strategy 1; Strategy 2 shown in Fig. 12(b) is designed by removing UAV 2 located in the center of the target area; In strategy 3, UAV 3 is removed, as shown in Fig. 12(c); Finally, UAV 5 is removed to form strategy 4 shown in Fig. 12(d). Then, the proposed system is successively applied to the above four scenarios, and its performance corresponding to different deployment strategies is evaluated with the expressions derived in Section III. During the simulation, the values of parameters other than the number and locations of UAVs are set according to Table I and remain constant. The performance evaluation results obtained are shown in Fig. 13.

The curves in Fig. 13(a) show that the proposed system's performance varies greatly among different deployment strategies. Strategy 4 (pink dash-dot line in Fig. 13(a)) exhibits the best position accuracy, and its corresponding 60% and 90% coverage RMSE is 16.2m and 18.9m, as shown in Fig. 13(b). For strategy 4 (blue dash line), its 60% and 90% coverage RMSE is 16.9m and 19.3m, which is very close to but slightly worse than that of strategy 2. The reason for the satisfactory performance of these two strategies is very clear, that is, the favorable geometry of anchor nodes. As can be seen from Fig. 12(b) and (d), for any sample point in the target area, strategy 2 and 4 could ensure that UAVs are approximately evenly distributed in azimuth, which is generally considered to be beneficial for positioning service. Compared with the two strategies mentioned above, the performance of strategy 1 and 3 is quite disappointing. In terms of strategy 3 (green solid line), it's 60% coverage RMSE is actually acceptable (17.7m), while the 90% coverage RMSE is 27.9m, which is almost 32.3% larger than that of strategy 2. The poor geometry of UAVs is the cause of this phenomenon. As shown in Fig. 12(c), for those sample points in the lower left corner of the target area, almost all UAVs are located on their right side, which commonly leads to large position errors. Finally, the 60% and 90% coverage RMSE of strategy 1 (yellow dash line) is 19.4m and 22.6m, which is about 16.5% and 16.4%

larger than the 16.2m and 18.9m for strategy 2. The reason for the poor performance of strategy 1 is quite similar to that explained in strategy 3.

From the above numerical results and analysis, it can be concluded that the UAV deployment directly determines the performance of the proposed system. In addition, adopting a good deployment strategy (strategy 4) could improve the position accuracy by about 16%, which is not much different from the effect brought about by adding one UAV. Therefore, in practical applications, the optimization of UAV deployment is also a promising way to improve the performance of the proposed system, which will be studied in our future work.

## V. CONCLUSION

In this article, we presented a novel UAV-assisted anti-jamming positioning system that could provide services for users in jamming environments. In the proposed system, multiple low-altitude UAVs first utilize ground reference stations to locate themselves, and then act as aerial anchor nodes to provide positioning services. We determined the structure and mathematical models of our system, and selected appropriate methods to support the UAV self-localization and positioning service. In order to evaluate the proposed system's theoretical performance, we further derive the CRLB for UAV self-localization and the RMSE of UE position estimate in the presence of jamming. In particular, the UAV position and clock uncertainty caused by jamming and noise are taken into account in the above derivation. Numerical results demonstrate that the proposed system can achieve a theoretical accuracy better than 20m in typical jamming scenarios, making it a promising alternative to existing positioning systems. We hope this article could lead to a new paradigm for the design of anti-jamming positioning systems.

## APPENDIX A
## MODEL OF DR-TWR TECHNIQUE

In this appendix, we introduce the DR-TWR protocol used in V2V links and derive its measurement model (equation (11)) [50]. As shown in Fig. 14, the DR-TWR corresponding to UAV pair $\langle V_n, V_i \rangle$ $(i \neq n)$ begins with a range request message send by UAV $V_n$. After detecting the request message, UAV $V_i$ first waits for $\tau_D$ seconds according to its local clock, and then sends back two response messages successively at
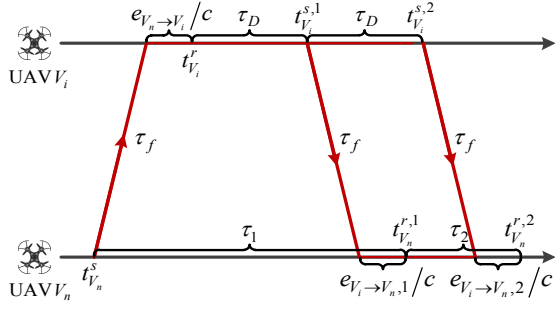
Fig. 14. Time diagram of DR-TWR.

an interval of $\tau_D$ seconds. UAV $V_n$ utilizes its local clock to measure the time interval $\tau_1$ between the transmission of request message ($t_{V_n}^s$) and the reception of the first response message ($t_{V_n}^{r,1}$), as well as $\tau_2$ between the receptions of two response messages ($t_{V_n}^{r,1}$ and $_{V_n}^{r,2}$). Denote the clock drifts of UAVs' local clocks relative to the reference clock as $\delta_{V_n}$ and $\delta_{V_1}$, then the measured time intervals ($\hat{\tau}_1$ and $\hat{\tau}_2$) can be expressed as [50]

$$\hat{\tau}_1 = t_{V_n}^{r,1} - t_{V_n}^s = 2\tau_f \cdot (1 + \delta_{V_n})$$
$$+ \left(\tau_D + \frac{e_{V_n \to V_i}}{c}\right) \cdot \frac{(1+\delta_{V_n})}{(1+\delta_{V_i})} + \frac{e_{V_i \to V_n,1}}{c}, \quad (62)$$

$$\hat{\tau}_2 = t_{V_n}^{r,2} - t_{V_n}^{r,1} = \tau_D \cdot \frac{(1+\delta_{V_n})}{(1+\delta_{V_i})} + \frac{e_{V_i \to V_n,2}}{c} - \frac{e_{V_i \to V_n,1}}{c}, \quad (63)$$

where $e_{V_n \to V_i} \sim \mathcal{N}\left(0, \sigma_{V_n \to V_i}^2\right)$, $e_{V_i \to V_n,1} \sim \mathcal{N}\left(0, \sigma_{V_i \to V_n}^2\right)$ and $e_{V_i \to V_n,2} \sim \mathcal{N}\left(0, \sigma_{V_i \to V_n}^2\right)$ are the ToA measurement errors caused by UAVs' internal noise and jamming; $\tau_f$ denotes the time-of-flight (ToF) between these two UAVs.

Then, the estimated ToF is given by [50]

$$\hat{\tau}_f = \frac{1}{2}(\hat{\tau}_1 - \hat{\tau}_2) = \tau_f \cdot (1 + \delta_{V_n}) + \frac{e_{V_n \to V_i}}{c} \cdot \frac{(1+\delta_{V_n})}{2(1+\delta_{V_i})}$$
$$+ \frac{e_{V_i \to V_n,1}}{c} - \frac{e_{V_i \to V_n,2}}{2c}. \quad (64)$$

Since the values of $\delta_{V_n}$ and $\delta_{V_i}$ are commonly very small in practice, the above equation can be rewritten as

$$\hat{\tau}_f \approx \tau_f + \frac{e_{V_n \to V_i}}{2c} + \frac{e_{V_i \to V_n,1}}{c} - \frac{e_{V_i \to V_n,2}}{2c}. \quad (65)$$

Therefore, the range measurement obtained by DR-TWR technique can be expressed as

$$r_{V_n \to V_i} = c \cdot \hat{\tau}_f = c \cdot \tau_f + \frac{e_{V_n \to V_i}}{2} + e_{V_i \to V_n,1} - \frac{e_{V_i \to V_n,2}}{2}$$
$$= r_{V_n \to V_i}^* + n_{V_n \to V_i}, \quad (66)$$

where $n_{V_n \to V_i} = \frac{e_{V_n \to V_i}}{2} + e_{V_i \to V_n,1} - \frac{e_{V_i \to V_n,2}}{2}$. Since the noise terms $e_{V_n \to V_i}$, $e_{V_i \to V_n,1}$ and $e_{V_i \to V_n,2}$ are independent of each other, the range measurement error $n_{V_n \to V_i}$ follows a zero-mean Gaussian distribution: $n_{V_n \to V_i} \sim \mathcal{N}\left(0, \frac{1}{4}\sigma_{V_n \to V_i}^2 + \frac{5}{4}\sigma_{V_i \to V_n}^2\right)$.

## REFERENCES

[1] H. Huang, G. Gartner, J. M. Krisp, M. Raubal, and N. Van de Weghe, "Location based services: ongoing evolution and research agenda," *Journal of Location Based Services*, vol. 12, no. 2, pp. 63–93, 2018.

[2] J. A. del Peral-Rosado, G. Seco-Granados, S. Kim, and J. A. Lpez-Salcedo, "Network design for accurate vehicle localization," *IEEE Transactions on Vehicular Technology*, vol. 68, no. 5, pp. 4316–4327, 2019.

[3] V. K. Yadav, S. Verma, and S. Venkatesan, "Efficient and secure location-based services scheme in VANET," *IEEE Transactions on Vehicular Technology*, vol. 69, no. 11, pp. 13 567–13 578, 2020.

[4] 3GPP TR 38.855, "Study on NR positioning support," Rel. 16, 2019.

[5] 6G Flagship, "Key drivers and research challenges for 6G ubiquitous wireless intelligence," Oulu, Finland, White Paper, 2019.

[6] D. Borio, F. Dovis, H. Kuusniemi, and L. Lo Presti, "Impact and detection of GNSS jammers on consumer grade satellite navigation receivers," *Proceedings of the IEEE*, vol. 104, no. 6, pp. 1233–1245, 2016.

[7] R. H. Mitch, R. C. Dougherty, M. L. Psiaki, S. P. Powell, B. W. O. J. A. Bhatti, and T. E. Humphreys, "Signal characteristics of civil GPS jammers," in *Proceedings of the 24th International Technical Meeting of the Satellite Division of The Institute of Navigation (ION GNSS 2011)*, 2011, pp. 1907–1919.

[8] Eurocontrol, "Eurocontrol voluntary ATM incident reporting (EVAIR) bullet in no 19. 2012-2016," 2018.

[9] K. Sun, M. Zhang, and D. Yang, "A new interference detection method based on joint hybrid time-frequency distribution for GNSS receivers," *IEEE Transactions on Vehicular Technology*, vol. 65, no. 11, pp. 9057–9071, 2016.

[10] R. Leandro, V. Gomez, R. Stolz, H. Landau, M. Glocker, R. Drescher, and X. Chen, "Developments on global centimeter-level GNSS positioning with trimble centerpoint RTXTM," in *Proceedings of the 25th International Technical Meeting of the Satellite Division of The Institute of Navigation (ION GNSS 2012)*, 2012, pp. 3089–3096.

[11] T. Suzuki, "Time-relative RTK-GNSS: GNSS loop closure in pose graph optimization," *IEEE Robotics and Automation Letters*, vol. 5, no. 3, pp. 4735–4742, 2020.

[12] D. Schmidt, K. Radke, S. Camtepe, E. Foo, and M. Ren, "A survey and analysis of the GNSS spoofing threat and countermeasures," *ACM Comput. Surv.*, vol. 48, no. 4, pp. 1–31, 2016.

[13] R. Morales-Ferre, P. Richter, E. Falletti, A. de la Fuente, and E. S. Lohan, "A survey on coping with intentional interference in satellite navigation for manned and unmanned aircraft," *IEEE Communications Surveys & Tutorials*, vol. 22, no. 1, pp. 249–291, 2020.

[14] L. Heng, T. Walter, P. Enge, and G. X. Gao, "GNSS multipath and jamming mitigation using high-mask-angle antennas and multiple constellations," *IEEE Transactions on Intelligent Transportation Systems*, vol. 16, no. 2, pp. 741–750, 2015.

[15] L. Zhang, L. Huang, B. Li, M. Huang, J. Yin, and W. Bao, "Fast-moving jamming suppression for UAV navigation: A minimum dispersion distortionless response beamforming approach," *IEEE Transactions on Vehicular Technology*, vol. 68, no. 8, pp. 7815–7827, 2019.

[16] M. Aghadadashfam, M. R. Mosavi, and M. J. Rezaei, "A new post-correlation anti-jamming technique for GPS receivers," *GPS Solutions*, vol. 24, 2020.

[17] K. Shamaei and Z. M. Kassas, "LTE receiver design and multipath analysis for navigation in urban environments," *NAVIGATION*, vol. 65, no. 4, pp. 655–675, 2018.

[18] M. Driusso, C. Marshall, M. Sabathy, F. Knutti, H. Mathis, and F. Babich, "Indoor positioning using LTE signals," in *2016 International Conference on Indoor Positioning and Indoor Navigation (IPIN)*, 2016, pp. 1–8.

[19] P. A. Zandbergen, "Accuracy of iPhone locations: A comparison of assisted GPS, WiFi and cellular positioning," *Transactions in GIS*, vol. 13, no. s1, pp. 5–25, 2009.

[20] M. Lichtman, R. P. Jover, M. Labib, R. Rao, V. Marojevic, and J. H. Reed, "LTE/LTE-A jamming, spoofing, and sniffing: threat assessment and mitigation," *IEEE Communications Magazine*, vol. 54, no. 4, pp. 54–61, 2016.

[21] Q. Liu, R. Liu, Z. Wang, and Y. Zhang, "Simulation and analysis of device positioning in 5G ultra-dense network," in *2019 15th International Wireless Communications & Mobile Computing Conference (IWCMC)*, 2019, pp. 1529–1533.

[22] Y. Zeng, R. Zhang, and T. J. Lim, "Wireless communications with unmanned aerial vehicles: opportunities and challenges," *IEEE Communications Magazine*, vol. 54, no. 5, pp. 36–42, 2016.

[23] X. Zhong, Y. Guo, N. Li, Y. Chen, and S. Li, "Deployment optimization of UAV relay for malfunctioning base station: Model-free approaches," *IEEE Transactions on Vehicular Technology*, vol. 68, no. 12, pp. 11 971–11 984, 2019.

[24] Y. Zhou, C. Pan, P. L. Yeoh, K. Wang, M. Elkashlan, B. Vucetic, and Y. Li, "Secure communications for UAV-enabled mobile edge computing systems," *IEEE Transactions on Communications*, vol. 68, no. 1, pp. 376–388, 2020.

[25] Y. Zhou, P. L. Yeoh, C. Pan, K. Wang, M. Elkashlan, Z. Wang, B. Vucetic, and Y. Li, "Offloading optimization for low-latency secure mobile edge computing systems," *IEEE Wireless Communications Letters*, vol. 9, no. 4, pp. 480–484, 2020.

[26] Z. Xiao and Y. Zeng, "An overview on integrated localization and communication towards 6G," *arXiv:2006.01535*, 2020.

[27] S. Zhang, Y. Zeng, and R. Zhang, "Cellular-enabled UAV communication: A connectivity-constrained trajectory optimization perspective," *IEEE Transactions on Communications*, vol. 67, no. 3, pp. 2580–2604, 2019.

[28] G. Han, J. Jiang, C. Zhang, T. Q. Duong, M. Guizani, and G. K. Karagiannidis, "A survey on mobile anchor node assisted localization in wireless sensor networks," *IEEE Communications Surveys & Tutorials*, vol. 18, no. 3, pp. 2220–2243, 2016.

[29] I. Ahmad, N. W. Bergmann, R. Jurdak, and B. Kusy, "Towards probabilistic localization using airborne mobile anchors," in *2016 IEEE International Conference on Pervasive Computing and Communication Workshops (PerCom Workshops)*, 2016, pp. 1–4.

[30] Z. Liu, Y. Chen, B. Liu, C. Cao, and X. Fu, "HAWK: An unmanned mini-helicopter-based aerial wireless kit for localization," *IEEE Transactions on Mobile Computing*, vol. 13, no. 2, pp. 287–298, 2014.

[31] A. Wang, X. Ji, D. Wu, X. Bai, N. Ding, J. Pang, S. Chen, X. Chen, and D. Fang, "GuideLoc: UAV-assisted multitarget localization system for disaster rescue," *Mobile Information Systems*, vol. 2017, 2017.

[32] H. Sallouha, M. M. Azari, A. Chiumento, and S. Pollin, "Aerial anchors positioning for reliable RSS-based outdoor localization in urban environments," *IEEE Wireless Communications Letters*, vol. 7, no. 3, pp. 376–379, 2018.

[33] H. Sallouha, M. M. Azari, and S. Pollin, "Energy-constrained UAV trajectory design for ground node localization," in *2018 IEEE Global Communications Conference (GLOBECOM)*, 2018, pp. 1–7.

[34] Z. Wang, R. Liu, Q. Liu, J. S. Thompson, and M. Kadoch, "Energy-efficient data collection and device positioning in UAV-assisted IoT," *IEEE Internet of Things Journal*, vol. 7, no. 2, pp. 1122–1139, 2020.

[35] I. Bisio, C. Garibotto, H. Haleem, F. Lavagetto, and A. Sciarrone, "On the localization of wireless targets: A drone surveillance perspective," *IEEE Network*, pp. 1–7, 2021.

[36] Z. Wang, R. Liu, Q. Liu, and L. Han, "Towards reliable UAV-enabled positioning in mountainous environments: System design and preliminary results," *arXiv:2009.04638*, 2020.

[37] F. Koohifar, I. Guvenc, and M. L. Sichitiu, "Autonomous tracking of intermittent RF source using a UAV swarm," *IEEE Access*, vol. 6, pp. 15 884–15 897, 2018.

[38] B. Park, D. Kim, T. Lee, C. Kee, B. Paik, and K. Lee, "A feasibility study on a regional navigation transceiver system," *The Journal of Navigation*, vol. 61, no. 2, pp. 177–194, 2008.

[39] C. He, B. Yu, and Z. Deng, "Wireless time synchronization for multiple UAV-borne pseudolites navigation system," in *China Satellite Navigation Conference (CSNC) 2016 Proceedings: Volume II*, 2016, pp. 303–315.

[40] M. Angjelichinoski, D. Denkovski, V. Atanasovski, and L. Gavrilovska, "Cramér-Rao lower bounds of RSS-based localization with anchor position uncertainty," *IEEE Transactions on Information Theory*, vol. 61, no. 5, pp. 2807–2834, 2015.

[41] F. K. W. Chan and H. C. So, "Accurate distributed range-based positioning algorithm for wireless sensor networks," *IEEE Transactions on Signal Processing*, vol. 57, no. 10, pp. 4100–4105, 2009.

[42] Z. Ma and K. C. Ho, "A study on the effects of sensor position error and the placement of calibration emitter for source localization," *IEEE Transactions on Wireless Communications*, vol. 13, no. 10, pp. 5440–5452, 2014.

[43] K. C. Ho, X. Lu, and L. Kovavisaruch, "Source localization using TDOA and FDOA measurements in the presence of receiver location errors: Analysis and solution," *IEEE Transactions on Signal Processing*, vol. 55, no. 2, pp. 684–696, 2007.

[44] A. Al-Hourani, S. Kandeepan, and A. Jamalipour, "Modeling air-to-ground path loss for low altitude platforms in urban environments," in *2014 IEEE Global Communications Conference*, 2014, pp. 2898–2904.

[45] H. Ren, C. Pan, K. Wang, Y. Deng, M. Elkashlan, and A. Nallanathan, "Achievable data rate for URLLC-enabled UAV systems with 3-D channel model," *IEEE Wireless Communications Letters*, vol. 8, no. 6, pp. 1587–1590, 2019.

[46] A. A. Khuwaja, Y. Chen, N. Zhao, M. Alouini, and P. Dobbins, "A survey of channel modeling for UAV communications," *IEEE Communications Surveys & Tutorials*, vol. 20, no. 4, pp. 2804–2821, 2018.

[47] K. N. R. S. V. Prasad, E. Hossain, and V. K. Bhargava, "Machine learning methods for RSS-based user positioning in distributed massive MIMO," *IEEE Transactions on Wireless Communications*, vol. 17, no. 12, pp. 8402–8417, 2018.

[48] K. N. R. Surya Vara Prasad, E. Hossain, and V. K. Bhargava, "Low-dimensionality of noise-free RSS and its application in distributed massive MIMO," *IEEE Wireless Communications Letters*, vol. 7, no. 4, pp. 486–489, 2018.

[49] R. Kaune, J. Hörst, and W. Koch, "Accuracy analysis for TDOA localization in sensor networks," in *14th International Conference on Information Fusion*, 2011, pp. 1–8.

[50] S. Frattasi and F. Della Rosa, *Mobile positioning and tracking: from conventional to cooperative techniques*. John Wiley & Sons, 2017.

[51] W. H. FOY, "Position-location solutions by Taylor-series estimation," *IEEE Transactions on Aerospace and Electronic Systems*, vol. AES-12, no. 2, pp. 187–194, 1976.

[52] 3GPP TR 23.724, "Study on Cellular Internet of Things (IoT) support and evolution for the 5G System," v16.0.0, Dec. 2018.

[53] D. Yang, Q. Wu, Y. Zeng, and R. Zhang, "Energy tradeoff in ground-to-UAV communication via trajectory design," *IEEE Transactions on Vehicular Technology*, vol. 67, no. 7, pp. 6721–6726, 2018.

[54] J. Zhang, Y. Zeng, and R. Zhang, "Spectrum and energy efficiency maximization in UAV-enabled mobile relaying," in *2017 IEEE International Conference on Communications (ICC)*, 2017, pp. 1–6.

[55] M. R. Gholami, R. M. Vaghefi, and E. G. Ström, "RSS-based sensor localization in the presence of unknown channel parameters," *IEEE Transactions on Signal Processing*, vol. 61, no. 15, pp. 3752–3759, 2013.

**Zijie Wang** received the B.S. degree in electrical and information engineering from Beihang University in 2017. He is currently pursuing the Ph.D. degree with the School of Electronic and Information Engineering, Beihang University, China. His current research interests include global navigation satellite system, terrestrial localization systems, indoor/outdoor seamless positioning, unmanned aerial vehicles, as well as the applications of these technologies to 5G and Internet of Things networks.

**Rongke Liu** (SM'19) is currently a Full Professor with the School of Electronic and Information Engineering, Beihang University. He received the support of the New Century Excellent Talents Program from the Minister of Education, China. He has attended many special programs, such as China Terrestrial Digital Broadcast Standard. He has published over 100 papers in international conferences and journals. His research interest covers wireless communication, channel coding, and aerospace communication.

**Qirui Liu** is currently pursuing the Ph.D. degree with the School of Electronic and Information Engineering, Beihang University, China.

**Lincong Han** is currently pursuing the Ph.D. degree with the School of Electronic and Information Engineering, Beihang University, China.

**John S. Thompson** (F'16) is currently a Professor at the School of Engineering in the University of Edinburgh. He specializes in antenna array processing, cooperative communications systems, energy efficient wireless communications and their applications. He has published in excess of three hundred and fifty papers on these topics. In January 2016, he was elevated to Fellow of the IEEE for contributions to antenna arrays and multi-hop communications. In 2015-2018, he has been recognised by Thomson Reuters as a highly cited researcher.